NC STATE UNIVERSITY

College of Sciences
Department of Marine Earth & Atmospheric Sciences

meas.ncsu.edu

Campus Box 8208
1125 Jordan Hall
2800 Faucette Drive
Raleigh, NC 27695-8208

Final Technical Report May 31, 2017

USGS Award Number: G15AP00091

Title of Award: *Establishing a High-Resolution Post-Glacial Chronology of Surface Rupture on the Lake Creek—Boundary Creek Fault, Puget Sound Region, Washington State*

Authors & Affiliations: Karl W. Wegmann[a], Elana L. Leithold[b], and DelWayne R. Bohnenstiehl[c]
Department of Marine, Earth, and Atmospheric Sciences
North Carolina State University
2800 Faucette Drive
Raleigh, NC 27695-8208

[a] E-mail: kwwegman@ncsu.edu; Tel: 919-515-0380; Fax: 919-513-8812
[b] E-mail: Leithold@ncsu.edu; Tel: 919-515-7282; Fax: 919-513-8812
[c] E-mail: drbohnen@ncsu.edu; Tel: 919-515-7449; Fax: 919-513-8812

Term Covered by Award: **Start:** July 1, 2015 **End:** February 28, 2017

Abstract: The Lake Creek–Boundary Creek fault and the Sadie Creek splay fault are similar to a number of steeply dipping crustal faults in the Puget Sound region exhibiting evidence for latest Pleistocene-Holocene surface rupture that accommodate north-south contraction and clockwise rotation of the Cascadia forearc in western Washington. The fault zone trends directly beneath Lake Crescent, which occupies a deep, glacially-scoured valley in Olympic National Park. There is direct physical evidence for surface ground rupture along at least 56 km of the fault zone both beneath Lake Crescent as well as to the west and east of the lake. Large Holocene landslide scarps surround the lake, and swath bathymetric data demonstrate that these failures deposited large masses of material into the lake itself. High resolution seismic reflection data and a suite of piston cores reveal that these landslides have produced four lake tsunami/seiche events during the past 8500 years, around 3100, 4000, 4900, and 7200 cal yr BP. When sediment core and seismic reflection data are combined, there is evidence to indicate that these events locally caused meters of erosion into the lakebed, and deposition of "megaturbidite" layers that are traceable over the entire 20 km^2 lake basin and exceed 1 m thickness over much of the deep lake floor. The megaturbidites consist of normally graded, faintly laminated sand overlain by thick, massive silt with dispersed plant debris, and clay caps. Petrologic data from the basal megaturbidite sands indicates that the sediment was derived from sources around the entire lake margin, as opposed to a single point source, and was likely remobilized from shallow subaqueous environments by the displacement waves. The c. 3100-yr BP megaturbidite deposit has an estimated volume of about 4.8 x 10^6 m^3. Preliminary modelling suggests that it was produced by an earthquake-triggered rockslide into the lake that likely generated a displacement waves with opposite-shore maximum run-up heights of 86 ± 17 m. The 3100-yr BP deposit has been undisturbed by subsequent events, but progressive deformation and offset of the three earlier megaturbidite layers visible in seismic reflection profiles indicates that their deposition is related to surface rupturing earthquakes on the Lake Creek – Boundary Creek fault zone. Based on evidence to date from Lake Crescent, the probability of a similar earthquake on the Lake Crescent segment of the fault zone in the next 50 years is estimated at about 5%.

Table of Contents:

Introduction

Research Motivation

Improving estimates of the sizes, recurrence intervals, and effects of late Quaternary earthquakes in the Puget Sound region, and evaluating earthquake-induced ground failure potential near bodies of water where landslides may generate local tsunamis are important for multiple reasons. First, this information bolsters our understanding of the regional seismic risk and to testing hypotheses related to seismic clustering along individual fault zones. Second, it provides insight into the potential for megathrust triggering of upper-crustal earthquakes above the Cascadia subduction zone in the greater Puget Sound region of Washington State (e.g., Gomberg and Sherrod, 2014; Sherrod and Gomberg, 2014). Earthquake-triggered mass wasting is an integral process for mass transfer and overall denudation in tectonically active settings (e.g., Keefer, 1984, 2002; Antinao and Gosse, 2009; Hovius et al., 2011; Parker et al., 2011). This processes is also an important mechanism for the short-to-long term impoundment of rivers, the rearrangement of drainage networks, and provides one mechanism for the genetic isolation of aquatic species (e.g., Mackey et al., 2011). In the Pacific Northwest, native oral traditions (legends) describing earthquakes, tsunamis, and large rock avalanches are not uncommon (e.g., Ludwin et al., 2007), and such events undoubtedly made lasting impressions on the witnesses, or those who later came upon the subsequently altered landscape (source).

Within this broader context, the specified goals of 2015-2017 USGS-NEHRP Grant G15AP00091 was to constrain the timing and recurrence interval of past earthquakes sourced from the Lake Creek – Boundary Creek fault zone (LCBCFZ), a 55-plus kilometer long upper crustal structure with previously demonstrated post-glacial (< ~ 14 ka) oblique slip and surface-rupturing earthquakes (Haugerud et al., 2002; Polenz et al., 2004; Schasse et al., 2004; Nelson et al., 2007). The Lake Crescent study site is located along the northern flank of the tectonically active Olympic Mountains and near to regional population centers (e.g. Port Angeles) and important transportation, utility and industrial corridors and facilities. Our proposal was motivated by four key observations: (1) prior seismic imaging illuminated up to 25 m of post-glacial sediment preserved within the deep basins of Lake Crescent; (2) along the trace of the

LCBCFZ beneath Lake Crescent, seismic imagery appeared to record repeat disruptions of lake sediments by earthquakes on the fault zone; (3) that the most recent of these earthquakes triggered one or more rock avalanches from the adjacent steep mountain sides above the lake; and (4) that this mass wasting into the lake likely generated displacement (tsunami) waves within the lake (Wegmann et al., 2014a). From these observations we proposed to collect three new data sets as an initial assessment of the timing and impacts of earthquakes and landslides triggered by the LCBCFZ at Lake Crescent that included: a high-resolution multi-beam bathymetric survey of Lake Crescent with partners from the USGS-Pacific Coastal Marine Science Center, sediment cores from Lake Crescent with partners from the National Lacustrine Core Facility (LacCore) at the University of Minnesota, and radiocarbon geochronology samples from the subaerial portion of mass wasting deposits between Lakes Crescent and Sutherland. This report documents the data sets that were collected and our preliminary interpretations of the timing of earthquakes and landslides generated by rupture of the LCBCFZ at Lake Crescent. It is also important to note that this USGS funding allowed for the research support of two Master of Science graduate students, Audrianna F. Pollen and Catelyn N. Joyner in the Department of Marine, Earth, and Atmospheric Sciences at NC State University who both completed their degree requirements and theses in 2016. Each of their M.S. theses on the paleoseismology of Lake Crescent is available to the public in downloadable Adobe PDF format from the North Carolina State University electronic repository for Theses and Dissertations at: https://repository.lib.ncsu.edu/handle/1840.20/23/discover.

Geologic Setting

Lake Crescent is located within the northern foothills of the Olympic Peninsula above the Cascadia subduction zone (CSZ) plate boundary (Fig. 1). The peninsula is bordered by the Strait of Juan de Fuca to the north and the Pacific Ocean to the west. The CSZ, located offshore in the Pacific Ocean, tectonically dominates the geology of the Pacific Northwest from northern California to Vancouver Island. The Olympic Mountains make up the subaerial portion of the Cascadia accretionary wedge that has formed in response to oblique subduction of the Juan de Fuca plate beneath the North American plate (e.g., Engbretson et al. 1985; Wells et al. 1998) at a Pliocene-to-modern rate of about 36 mm/yr (DeMets and Dixon, 1999).

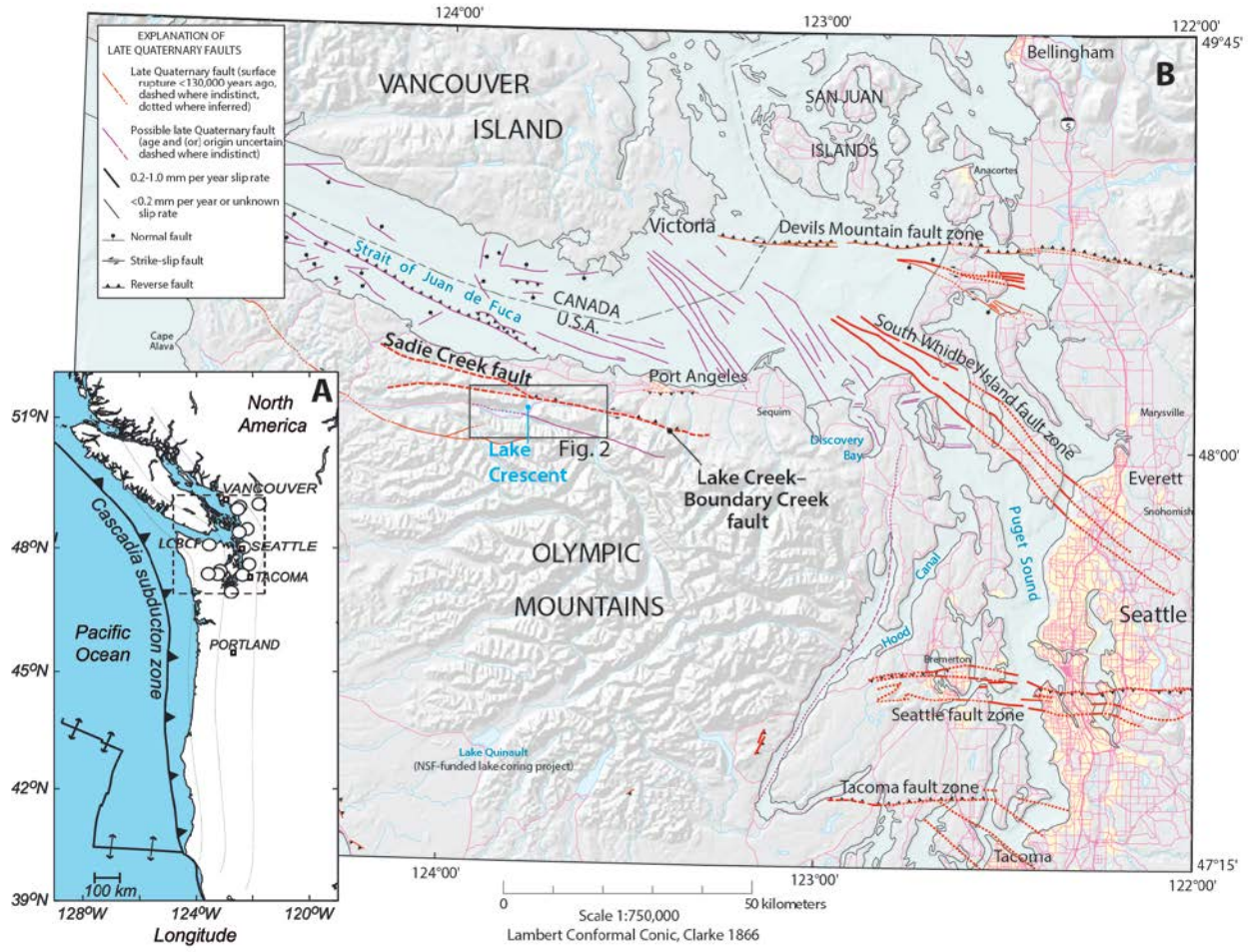

Figure 1. Active tectonics of the Cascadia margin. **A**. Map of the Cascadia subduction zone showing locations of known late Holocene upper plate earthquakes (open circles), modified from Sherrod & Gomberg (2014). Dashed rectangle shows location of enlarged map. **B**. Map of the northwest Washington State showing known and possible late Quaternary faults from Lidke et al. (2003) (2004). Study area along the Lake Creek-Boundary Creek fault zone in the vicinity of Lake Crescent outlined by rectangle. Figure modified from Nelson et al. (2007).

The estimated 36 mm/yr rate of convergence and clockwise vertical-axis rotation of the northwestern Washington forearc against the more rigid Coast Mountain buttress of southwestern British Columbia has resulted in a large, east-plunging anticline composed of deformed Tertiary marine volcanic and sedimentary units beneath the Olympic Peninsula (Tabor and Cady, 1978a, b; Engbretson et al. 1985; Brandon and Calderwood, 1990; Clowes et al. 1997; Wells et al., 1998; Wells and Simpson, 2001; Fig. 2). Fine and coarse marine

sedimentary units known as the Olympic Subduction Complex (OSC) compose the core of the Olympic Mountains. The OSC is bounded by the Hurricane Ridge Fault and flanked by Paleocene-to-Eocene marine basalt and sedimentary rocks of the Crescent Formation (Tabor & Cady, 1978a, b; Engbretson et al. 1985; Brandon and Calderwood, 1990; Clowes et al. 1996; Brandon et al. 1998) and younger sedimentary sequences (Schasse, 2003; Fig. 2). The Olympic Mountains are considered to be in a flux steady state, meaning that the rate of the material accreted into the subduction complex is balanced by the volume of material eroded from the surface (Brandon et al. 1998; Pazzaglia and Brandon, 2001; Willet and Brandon, 2002).

Figure 2. Location of the Lake Creek–Boundary Creek fault (from Brown et al., 1960; Tabor & Cady, 1978; Polenz et al., 2004; Schasse et al., 2004) and the Sadie Creek fault (Joyner, 2016), a previously unnamed splay fault of the LCBCF first mapped by Brown et al. (1960). Paleoseismic excavations across the eastern LCBC fault by Nelson et al. (2007; in press) are shown as thick yellow lines that these authors named the Daisy (A), Corners and Microcorners (B), Sapsucker (C), and Knee-high (D) trenches, respectively (see Fig. 21, this proposal). Rectangle shows bounds of Figures 3 and 4.

The northern Olympic Peninsula was at times extensively glaciated during the Quaternary. The foothills and lowlands flanking the saltwater were buried beneath the ~1 km thick Juan de Fuca lobe of the Cordilleran ice sheet as recently as ~14 ka (Dethier et al. 1995; Polenz et al., 2004; Wegmann et al., 2012). The valley occupied by Lake Crescent was almost certainly over-deepened by erosion of the Juan de Fuca lobe as it advanced and retreated

across the study area (Tabor, 1975). In the vicinity of Lake Crescent, the late Quaternary glacial advances and retreats deposited till, outwash, and glaciolacustrine terrace deposits along adjacent valley floors and walls (Heuser, 1973; Schasse, 2003; Fig. 2).

Researchers have developed kinematic models for the Cascadia forearc based upon paleomagnetism, observations of fault displacements, and GPS geodesy that partitions the forearc into a series of ridged clockwise-rotating blocks driven by rotation from Pacific-North America shear and extension in the Basin and Range (Wells et al., 1998; Wells and Simpson, 2001; Wells and McCaffrey, 2013). This clockwise rotation causes higher rates of convergence in western Washington than elsewhere in Cascadia as the Oregon Coast Range Block impinges on Tertiary volcanic and sedimentary rocks (e.g. the Olympic Subduction Complex and Crescent Formation) against the southern edge of the British Columbia Coast Mountains, resulting in uplifted blocks separating structural basins (Fig 1; e.g. Brocher et al., 2001). Geodetic studies demonstrate that the Olympic Peninsula and Puget Sound region experiences north-south contraction averaging ~3 to 4.4 mm/yr that decreases to near zero in southern British Columbia (Wells et al., 1998; Mazzotti et al., 2002; Hyndman et al., 2003; McCaffrey et al., 2007). The Lake Creek–Boundary Creek fault zone is one of three major, east-west-trending, north-dipping faults on the north flank of the Olympic Mountains that appears to accommodate a portion of both the clockwise rotation of northwestern Washington and north-directed contraction through oblique right-lateral slip at least in part during discrete earthquake events (Nelson et al., 2007; Joyner, 2016; Pollen, 2016; Nelson et al. (in press); Fig. 1 & 2). In addition to the Lake Creek-Boundary Creek fault zone, the Barnes Creek, and Hurricane Ridge faults have also accommodated north-south convergence (Tabor and Cady, 1978a; Schasse, 2003; Fig. 2). At present it is unknown if either of these other faults have generated surface-rupturing earthquakes since deglaciation. High resolution lidar topographic data along these faults has not yet been collected because they lie predominantly in unpopulated valleys within the boundaries of Olympic National Park.

Lake Creek–Boundary Creek Fault Zone

Herein we briefly describe the fault naming conventions used in this report in the context of previous research on the Lake Creek–Boundary Creek fault zone and its recently

appreciated role in accommodating active northward convergence and clockwise rotation of the northwestern Washington forearc. In the vicinity of Lake Crescent, geologic maps of the northern Olympic Peninsula document four north-dipping faults trending east-west between the northern foothills of the Olympic Mountains and the Strait of Juan de Fuca, which from south to north are the (1) Hurricane Ridge, (2) Crescent (also named Barnes Creek), (3) Lake Creek – Boundary Creek, and (4) Lower Elwha faults (Figs. 1, 2; Schasse and Wegmann, 2000; Dragovich et al., 2002; Schasse, 2003; Polenz et al., 2004; Schasse et al., 2004). The Lake Creek – Boundary Creek fault occupies a nearly continuous, structurally-controlled, east-west trending topographic valley parallel to the front of the Olympic Mountains (Fig. 2). It was first mapped by Brown et al. (1960) as two separate faults; the Boundary Creek fault west of Lake Crescent and the Lake Creek fault south and east of Port Angeles. On their geologic map of the Olympic Mountains, Tabor and Cady (1978a) inferred that the Boundary Creek and Lake Creek faults of Brown et al. (1960) represented a continuous, through going structure that in 2004 Polenz et al. and Schasse et al. termed the Lake Creek-Boundary Creek fault based in part on numerous offsets of late Pleistocene and Holocene deposits and landforms identified from both lidar data (e.g. Haugerud et al., 2003) and field observations (Nelson et al., 2007; in press). Brown et al. (1960) identified a northwest-trending splay fault that merges into their Boundary Creek fault beneath Lake Crescent; however this fault remained unnamed until 2016. Wegmann et al. (2014a, b) documented from seismic reflection data that the Holocene sedimentary infill of Lake Crescent was disturbed and offset along the traces of both the Lake Creek – Boundary Creek and northwest trending splay fault and Joyner (2016) named this splay the Sadie Creek fault based upon evidence of topographic offset of geomorphic surfaces visible in lidar data to the west of Lake Crescent, which were confirmed by Nelson et al. (in press). In this report we refer to the Lake Creek – Boundary Creek fault zone at Lake Crescent as including both the main east-west trending structure as well as the Sadie Creek splay fault (Figs 2, 3). Collectively, the LCBCFZ encompasses an east-west trending system of structures with at least 55 km of documented late Pleistocene-to-Holocene surface rupture from ca. 40 km east of Lake Crescent on the Lake Creek – Boundary Creek fault to 15 km west of the lake on the Sadie Creek fault (e.g. Haugerud et al. 2003; Schasse et al., 2004; Polenz et al., 2004;

Nelson et al., 2007; Joyner, 2016; Nelson et al., in press).

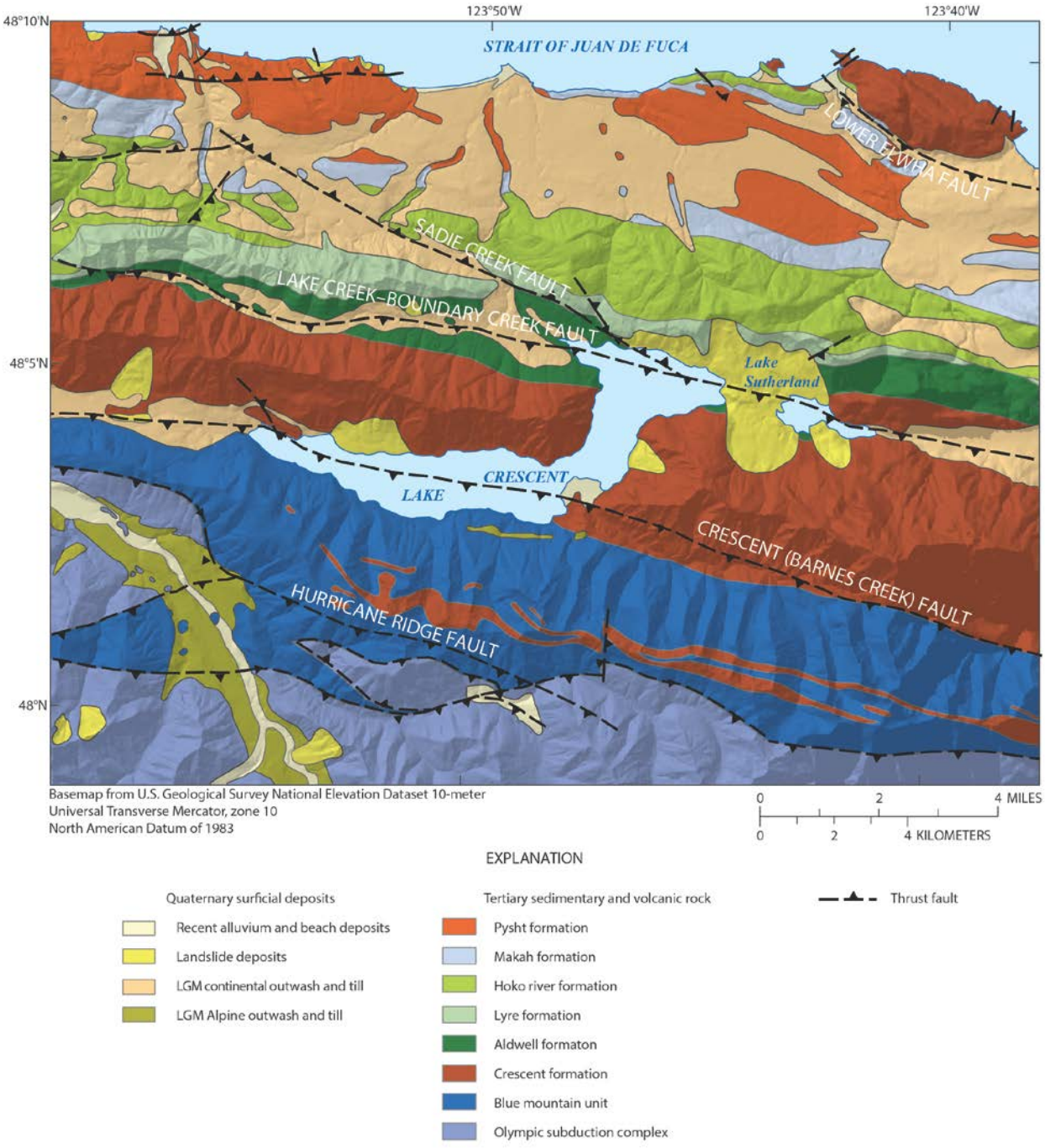

Figure 3. Geologic map of the Lake Crescent area of the north Olympic Peninsula, Clallam County, Washington. Modified from Schasse (2003) and Moran et al. (2012).

The Lake Creek-Boundary Creek fault zone exhibits oblique right-lateral dip slip motion, as is supported by lidar mapping, fault trenching, and field mapping (Brown et al. 1960; Tabor and Cady, 1978a,b; Schasse, 2003; Polenz et al. 2004; Schasse et al. 2004, Nelson et al. 2007; in press; Fig. 3). Fault scarps preserved in the landscape east of the Elwha River were used to estimate that the Lake Creek-Boundary Creek fault post-dated regional glaciation (< c. 13 ka) (Haugerud, 2002; Polenz et al. 2004; Schasse, 2004). Polenz et al. (2004) observed fault scarps on outwash terraces deposited c. 13 ka but not in late Pleistocene alluvium that was deposited just after the outwash terraces and from this evidence concluded that the last rupture along the fault in the vicinity of the Elwha River (~ 15 km east of Lake Crescent) was shortly after deglaciation. Fault scarps west of the Elwha River associated with the Lake Creek-Boundary Creek fault could not be accurately distinguished from widespread valley-margin landslide scarps, but surface faulting, visible in lidar imagery east of the Elwha River extends for 22 km (Polenz et al. 2004; Nelson et al. 2007).

Fault trenching east of the Elwha River produced radiocarbon evidence that suggests two surface- rupturing earthquakes have occurred in the past c. 3,000 years, one at 1,300 and another at 2,900 cal yr BP (Fig. 2; Nelson et al. 2007; in press). In addition, two older earthquakes are tentatively identified in the trench records, indicating a third event occurred sometime between 5 and 8 ka, with the possibility of a fourth event between 8 and 12 ka (Nelson et al., 2007; in press). The existence of surface faulting associated with the Lake Creek-Boundary Creek fault west of the Elwha River was not confidently identified until 2015 lidar imagery revealed topographic lineaments (inferred scarps) west of Lake Crescent's northern basin along the Sadie Creek fault (Fig. 4). The right-lateral motion shown by the offset drainage pattern of small stream valleys indicates the western half of the Lake Creek-Boundary Creek fault and the Sadie Creek fault zone is active and has generated surface-rupturing earthquakes west of, and most likely beneath the northern portion of Lake Crescent since regional deglaciation c. 14 ka (Joyner, 2016).

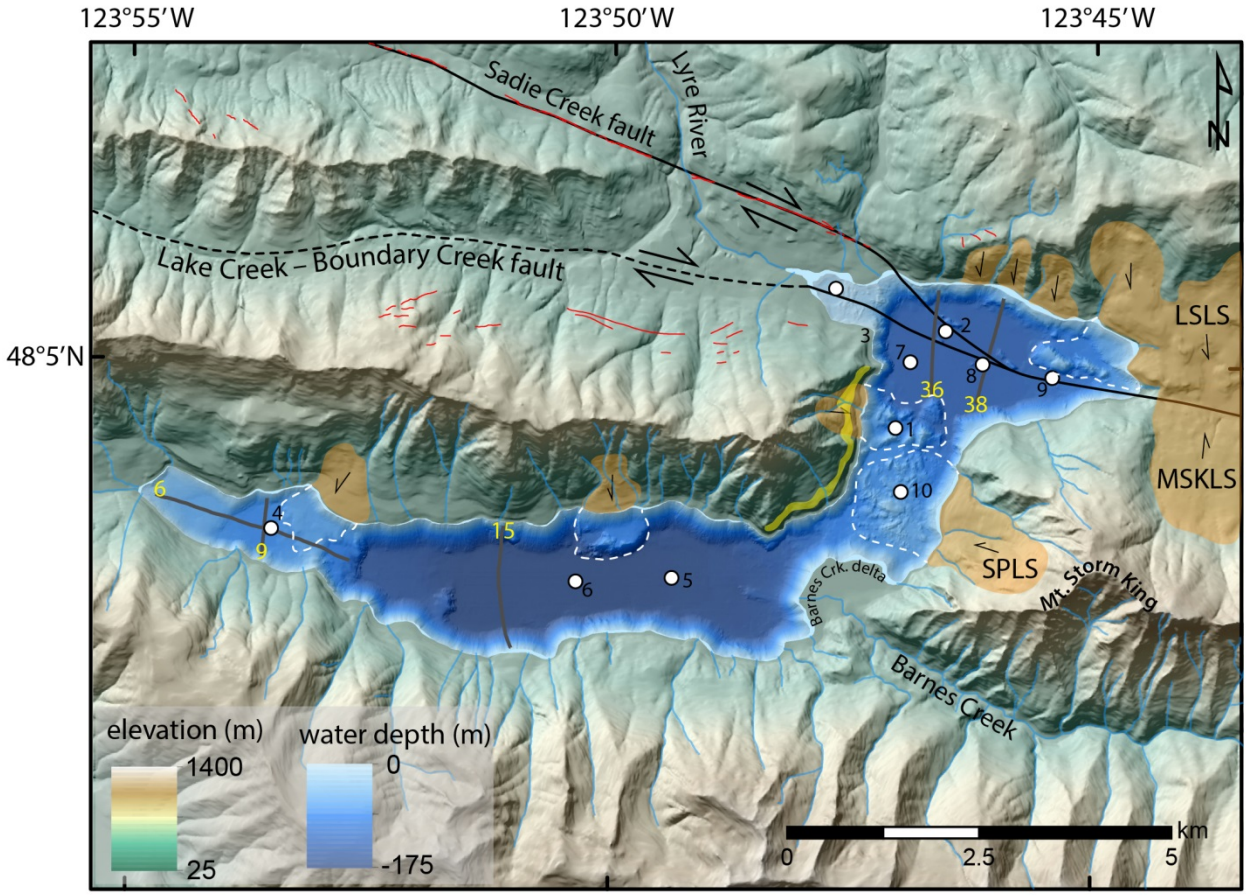

Figure 4. Topographic and bathymetric map of the Lake Crescent study area. Selected Chrip seismic reflection lines are shown as gray lines with yellow numbering. Sediment cores sites from 2015 are identified as white circles with black numbering. Surface rupture and topographic lineaments identified from 2015 lidar (Washington State Dept. of Natural Resources) are shown as thin red lines over the trace of the Sadie Creek fault and near to the trace of the Lake Creek–Boundary Creek fault. Large landslides (shown in orange) with runouts into the lake are identified as the Sledgehammer Point (SPLS), Mount Storm King (MSKLS) and Lake Sutherland (LSLS) complexes. We propose that the SPLS was triggered by the most recent earthquake of the LCBCFZ in the vicinity of Lake Crescent c. 3,100 cal yr BP and is believed to be the cause for Megaturbidite A. The yellow-shaded region across from the SPLS is the estimated 80±20 m high displacement wave run-up height based upon landslide volume entering the lake (Joyner, 2016).

Lake Crescent Catchment

Lake Crescent is a deep, ultra-oligotrophic, glacially-carved lake at the northern boundary of Olympic National Park. The 20.3 km^2-lake is composed of two elongated basins connected across a bathymetric sill (Figure 4). The east-west trending basins are characterized

by steep slopes that lead to flat bottoms whose depths are 140 m in the north and 190 m in the south. A small sub-basin exists in the western part of the south basin, where a bathymetric sill separates it from the deeper main southern basin (Fig. 4). The bathymetric sill between the two is thought to be a recessional glacial moraine that formed during regional retreat of the Juan de Fuca lobe of the Cordilleran ice sheet, approximately 14 ka (Logan and Schuster, 1991; Polenz et al. 2004; Wegmann et al., 2012). Lake Crescent is surrounded by steep, forested slopes underlain by igneous and sedimentary rocks of the Eocene Crescent, Hoko River, Lyre, and Aldwell formations (Fig 3). Mapped rockslide deposits within the Lake Crescent catchment total 11.3 km^2, or about 10% of the catchment surface area. Bathymetric surveys of the lake as part of this project revealed large subaqueous rockslide deposits in addition to the previously-identified subaerial portions (Fig 4). The largest landslide, herein named the Lake Sutherland rockslide complex, split ancestral Lake Crescent into two lakes, Crescent and Sutherland (Tabor, 1975; Logan and Schuster, 1991; Fig. 3; Fig. 5). Landslides from both the north and south valley walls culminated in the blockage of the ancestral outlet of Lake Crescent from the eastward flowing Indian Creek to the north flowing Lyre River. In addition, the rockslide dam caused the surface water elevation of Lake Crescent to increase by 24 m (elevation difference between the heads of Indian Creek and the Lyre River) as well as the genetic isolation of rainbow and cutthroat trout in Lake Crescent (Pierce, 1984; Meyer and Fradkin, 2002; Brenkman et al. 2014). The Lake Sutherland rockslide complex was previously estimated by Pringle et al. (2010) to have occurred around 4,340 ± 50 years ago by radiocarbon dated growth rings in a preserved, submerged, and drowned tree at the west end of the lake's south basin. An older mass wasting event, known as the Mount Storm King rockslide (Fig. 3; Fig. 5), was sourced off the north flank of this mountain. Preliminary radiocarbon dating of sediments accumulated in a closed depression formed on the top of this rockslide indicates that it occurred prior to 5,180 cal yr BP (see results section), and thus the re-routing of the outlet for Lake Crescent to the Lyre River likely occurred between c.4 to 5 ka. As discussed below, the Sledgehammer Point rockslide (Joyner, 2016) entered Lake Crescent around 3000 years ago, and its deposits are evident today as the bathymetric sill separating the deep southern and northern basins of the lake (Fig. 3).

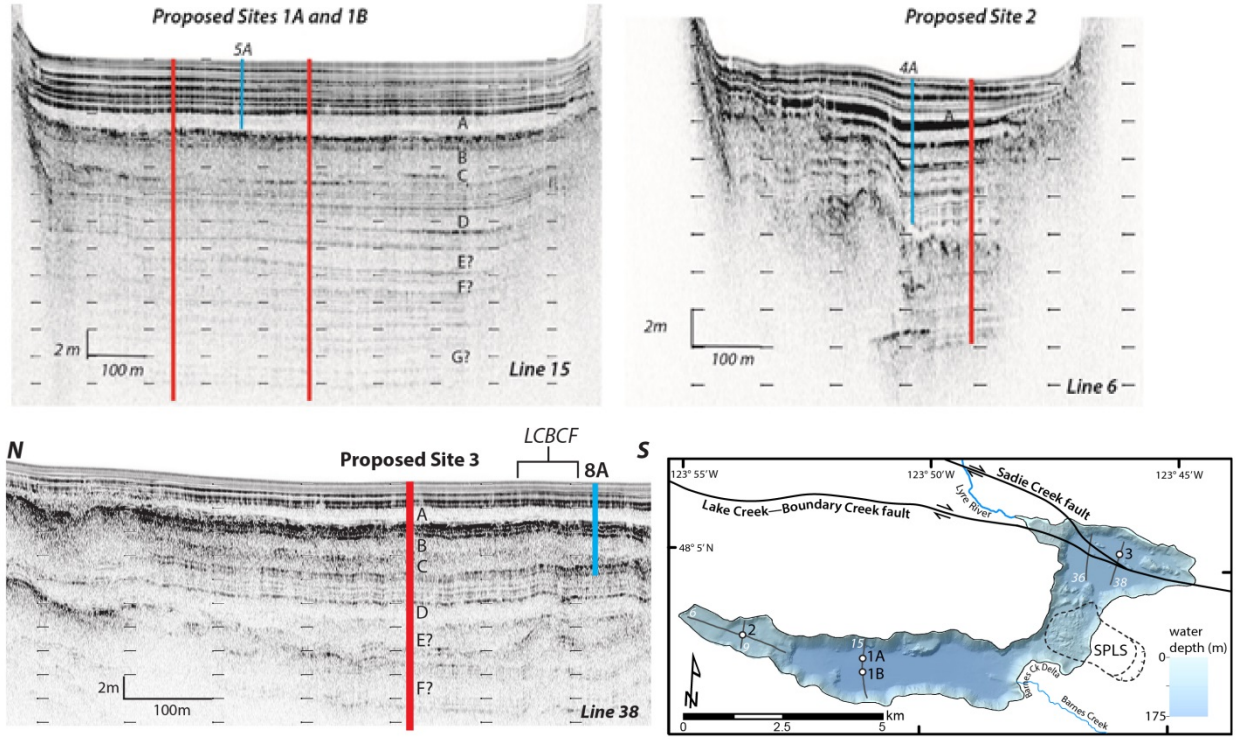

Figure 5. Select Chirp seismic reflection profiles from Lake Crescent showing location and sampling depth of piston cores acquired in 2015 as a part of this NEHRP-funded research project (blue lines). Red lines indicate our hope to acquire longer, repeat-drive percussion piston cores in the near future to lengthen the paleoseismic record from Lake Crescent and of the proposed repeat-drive percussion piston cores (red lines). Letters A-D denote megaturbidites sampled and dated in our 2015-funded NEHRP study, while E-G are additional megaturbidites tentatively identified in the seismic profiles.

Oral traditions of Pacific Northwest Native American tribes reveal an interesting backstory to the Mount Storm King rockslide. Clark (1953) describes a battle between the Klallam and Quillayute peoples near the shores of the Strait of Juan de Fuca. After two days of fighting and countless deaths, an infuriated Mount Storm King broke off a great piece of rock from his head and threw it down into the valley killing all of the warriors and splitting the lake in two (Clark, 1953). Although the story is but a legend, its existence does strengthen the evidence that landslides around Lake Crescent have occurred in the late Holocene and likely were witnessed by local inhabitants.

Earthquake disturbance at Lake Crescent

Our work in Lake Crescent has revealed evidence for at least four episodes of post-

glacial earthquake disturbance attributable to ruptures of the LCBCFZ. Our investigation of Lake Crescent began in 2013, as an extension of an unrelated project, when we collected ~75 km of exploratory CHIRP seismic imagery using an Edgetec CB-512i system towed near the surface using a small catamaran system deployed behind a 17' motorboat (Wegmann et al., 2014a). Seismic stratigraphy was apparent to the limits of acoustic penetration, up to 26 m depths beneath the lake bottom (Fig 5). From the seismic data set, two key observations motivated us to submit a proposal to NEHRP for further research in Lake Crescent. First, we observed a thick (1-2 m), acoustically transparent unit (labeled A in Figs. 5 and 6) visible at around 2-3 m beneath the current lake floor and present across the entire lake that we hypothesized to be a mass wasting deposit. Second, we observed that where the acoustically transparent unit lies atop the trace of the LCBC and the Sadie Creek splay fault, it is virtually undeformed and in turn is overlain by undeformed sediments (Fig. 6). At greater depth in the lakebed, however, three to four units of similar seismic appearance are cut by the fault and with increasing depth, each of them show evidence for progressively greater deformation (Fig. 6). Based on these observations, we hypothesized that the LCBCFZ has ruptured repeatedly in the past thousands of years and has triggered rock avalanches and landslides into the lake and the deposition of widespread event deposits.

Methods

Multibeam Bathymetry

A high resolution bathymetric survey of Lake Crescent was conducted in February 2016 by the crew of the U.S. Geological Survey's *R/V Snavely* operating a 100 kHz Reson 7111 multibeam system that returns both bathymetry and back-scatter intensity with individual beam arcs of 1.9° along-track and 1.5° across-track (Fig. 6). Data (pixel resolution ~2.5 m) were collected over swath widths three times the water depth at speeds of <5 nm/hr and the survey tracks were positioned with at least 25% overlap. Differentially corrected GPS navigation data was passed through an inertial measurement unit to the system hardware and data collection software. The multibeam data was post-processed by scientists at the USGS – Pacific Coastal Marine Science Center (PCMSC) into a georeferenced ArcGIS raster file with 3 m grid spacing. Finalized data will be made available to the public via the PCMSC web data

portal [https://walrus.wr.usgs.gov/data.html] following the completion of USGS quality assurance and control protocols.

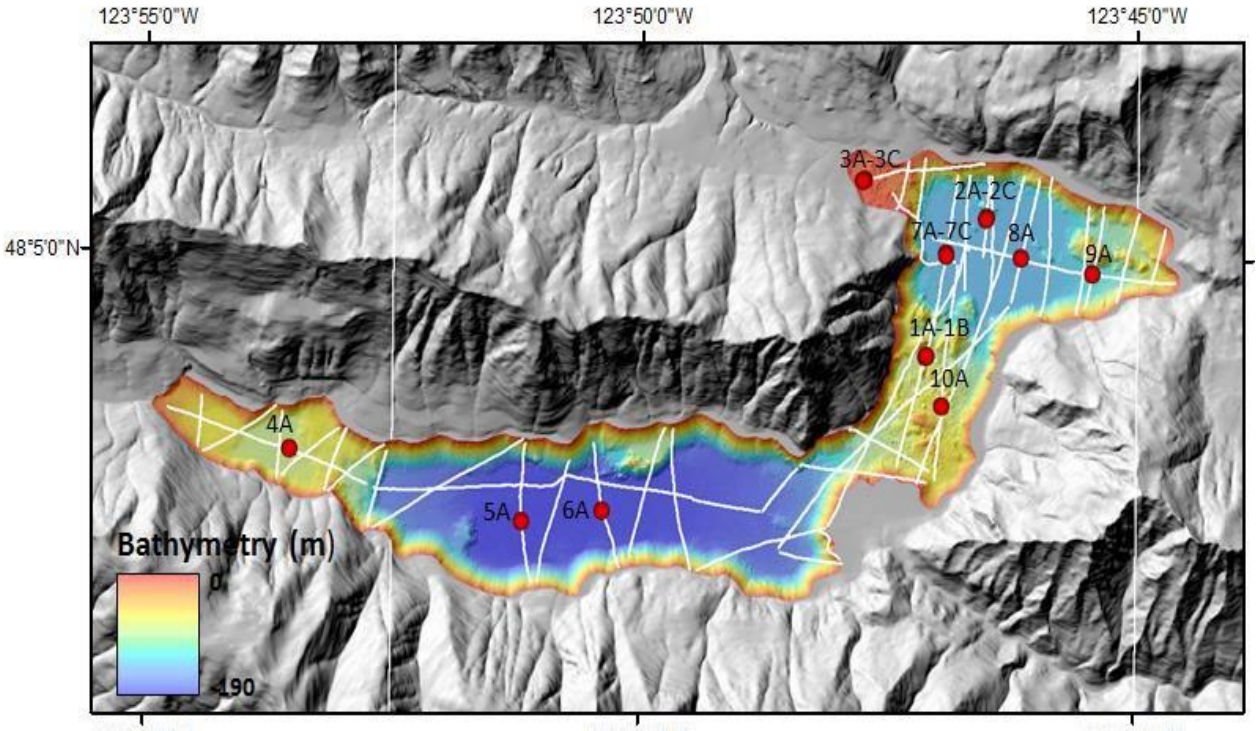

Figure 6. 2013 Chirp seismic survey (white lines) and 2015 core locations and names (red). The 3 m resolution bathymetric map is surrounded by 10 m DEM topography (USGS, 2001).

Lake Coring

In the Fall of 2015, funded by this grant from NEHRP, cores ranging from 4-8 m in length were recovered from 10 sites in Lake Crescent (Fig. 6) using both gravity and Kullenberg piston coring systems (Kelts, 1986) deployed from a specially constructed floating platform, the R/V KRKII (Fig. 7), and operated in partnership with personnel from LacCore, the National Lacustrine Coring Facility. The metal core barrels were lined with 7 cm diameter polycarbonate tubes. The Kullenberg cores ranged in total length from 0.41 to 7.90 m (Table 1) and the gravity cores ranged from 0.09 to 0.55 m long. The gravity cores were recovered to retrieve intact shallow sediments that otherwise could be disturbed during the piston coring process. A gravity core was not extracted from each piston core site. In addition, some of the gravity cores were not recovered simultaneously with the piston cores

due to mechanical malfunction and sediment consistency of the lake bottom. It is important to note that an undetermined amount of core 2A-1K may have been lost due to the lack of a core catcher at the end of the barrel. The upper two-thirds of core 7A-1K was disturbed upon on-shore extraction from the metal casing. All cores were capped, labeled, sealed, and transported to LacCore where they were placed in refrigerated storage.

Figure 7. Aerial view of the LacCore Kullenberg sediment coring platform R/V KRKII in September, 2015. Note people (8 total) on deck for scale.

Table 1. Lake Crescent core IDs, length, water depth at core site, and location.

Core ID (SHAKE-CRSC15-)	Core Length (m)	Water Depth (m)	Latitude	Longitude
1A-1K	1.07	83	48.073713	-123.785547
1B-1K	2.18	83	48.073817	-123.785367
2A-1K	5.31	140	48.0875	-123.775433
2C-1K	6.75	140	48.087383	-123.77555
3A-1K	0.41	20	48.091105	-123.795898
3C-1K	2.63	20	48.091083	-123.796233
4A-1K	7.85	83	48.06375	-123.892283
5A-1K	4.86	179	48.056883	-123.8532
6A-1K	5.36	179	48.058	-123.839617
7A-1K	6.74	141	48.083917	-123.782217
7C-1K	6.53	141	48.083733	-123.7821
8A-1K	7.90	140	48.083533	-123.76965
9A-1K	2.05	125	48.08205	-123.757583
10A-1K	0.99	66	48.068633	-123.782717

Core Sediment Properties and Geochronology

Within a few weeks of collection, members of our team processed the cores at the LacCore facility at the University of Minnesota. Whole core segments were scanned on a Geotek Standard Multisensor Core Logger (Geotek Limited, Daventry, UK) to measure bulk sediment density, acoustic wave velocity, electrical resistivity, and magnetic susceptibility at 5 mm resolution. The cores were then split and the sediment surface was cleaned with glass plates in preparation for imaging and description. Cores images were generated on a Geotek Geoscan-IV linescan camera mounted on a dedicated MSCL-CIS track, and the core halves were scanned on a Geotek XYZ Multisensor Core Logger for color spectrophotometric reflectance and high-resolution point sensor magnetic susceptibility at 5 mm resolution. The core lithologies were then described and sampled, including for plant macrofossil material to be used for AMS-^{14}C analyses to construct core age-depth models. The photos and initial descriptions were later used to tally and describe event layer thicknesses. Elemental distributions for cores 2C, 4A, and 6A were generated using an ITRAX micro-XRF scanner at the Large Lakes Observatory in Duluth, Minnesota. The cores were scanned by a Mo X-ray tube with a 2 mm sampling step and a 30 second dwell time.

Samples taken from the cores were transported to North Carolina State University and frozen until further analysis. The particle size distribution of thawed samples was characterized using a Beckman Coulter LS13-320 Laser Diffraction Particle Size Analyzer equipped with a Universal Liquid Module. The instrument measures particle size between 0.04 and 2000 microns. Plant debris, including twigs, bark, leaf fragments, needles, and roots were sampled from cores 2 through 9 and were analyzed for radiocarbon (^{14}C) at Direct AMS in Seattle, Washington and NOSAMS in Woods Hole, Massachusetts. Prior to submission for analysis, the samples were cleaned with 1N HCl and NaOH (the ABA method; Olsson, 1986) to remove any carbonate coatings or humic acids that may have contaminated them during burial in soils or the lake bed. OxCal 4.2 software (Bronk Ramsey, 2009) was used to calibrate the results with the IntCal13 calibration data of Reimer et al. (2013).

Landslide and Megaturbidite Volume Calculations and Displacement Wave Height Estimation

Volume estimation of the Sledgehammer Point rockslide (Joyner, 2016) was executed in ArcGIS ArcMap 10.3.1 using spatial data projected into the UTM Zone 10, WGS 1984 coordinate system. First, the area (m^2) of the mapped rockslide polygon was calculated. Next, the predicted volume of a given rockslide area was estimated by a bedrock rockslide geometry scaling relationship derived from Larsen et al. (2010) using a scaling exponent γ = 1.35 and intercept α = 0.186 such that $V = \alpha A^{\gamma}$. These scaling values were chosen because the area of the rockslide is > 5,000 m^2 (Larsen et al. 2010) and the assumed failure plane is tens of meters beneath the pre-failure ground surface.

The volume of the subaqueous portion of the Sledgehammer Point rockslide was completed by first establishing points that surround the rockslide debris using the 3 m resolution bathymetric raster as a reference. Bathymetric raster values were assigned to the points using the *Extract Values to Points* tool. The points were interpolated using the ordinary kriging method with a K-bessel model type within the ArcGIS Geostatistical Wizard in order to produce a raster of the pre-rockslide lake bathymetry. The kriging prediction map was converted to a raster using the *Layer to Grid* tool in Geospatial Analyst. Next, the points were used to make a polygon shapefile enclosing the rockslide debris. The 3 m resolution bathymetric and kriging rasters were extracted by mask to the shape of the polygon. The kriging raster was subtracted from the 3 m resolution bathymetric raster using the raster calculator tool and then multiplied by its cell resolution. The multiplied raster and rockslide debris polygon was input into the *Zonal Statistics as Table* tool, producing a data table in which the "sum" category represents the volume of the multiplied raster in m^3.

The volume of the first distinctive, acoustically transparent layer (layer A in Figures 5 and 6) observed beneath the lake bed in the Chirp seismic reflection data was estimated by a series of steps using various software packages. High resolution seismic reflection surveys of the sub-bottom lake stratigraphy were generated using the default JSF files generated by the Edgetech Discover SB 3200-XS program. The seismic reflection surveys were converted to standard SEG-Y IBM Floats (1) ASCII format. The SEG-Y files were imported to HYPACK 2016 for digitization of the layers seen in the sub-bottom stratigraphy. The elevation of the lake bed

was calculated by manually picking out the sediment-water interface in the seismic reflection surveys with the assumption that the freshwater seismic velocity is 1500 m/s. The acoustically transparent layer was digitized by tracing a reflector above and below the seismically transparent portion of the layer. Each reflector was traced by georeferenced points and exported as individual reflector ACSII X,Y,Z text files containing values of easting, northing, depth, and thickness for each digitized point.

MATLAB R2014a was utilized to produce a script that interpolated the thickness of the layer between the manually picked points (Appendix D of Joyner, 2016). First, the ACSII X,Y,Z text files were imported into MATLAB and easting and northing was converted to latitude and longitude. The latitude and longitude of the top and bottom reflectors were interpolated with the new line lengths dependent upon the bottom reflector length. The thickness was predicted for both reflectors given their individual latitude and longitude distances, depth of points, and interpolated distance points. Finally, the predicted thickness of the top reflector was subtracted from the predicted thickness of the bottom reflector to give a final interpolated data set of latitude, longitude, and thickness (X,Y,Z) for each Chirp line.

The Chirp X,Y,Z data were imported into ArcGIS ArcMap 10.3.1 to create isopach maps of megaturbidite layers A, B, C, and D and to estimate their volumes. The projected coordinate system used was WGS 1984 UTM Zone 10. The Chirp data were separated into three sections: north basin, south basin, and the small western extension of the south basin. The following procedure was executed for the three basins. First, zero points were made outlining the basin shape where X,Y,Z data existed. The points were georeferenced and then converted to a polygon shapefile. A new .csv file of georeferenced zero and Z points was interpolated using the ordinary kriging method with a K-bessel model type available in the Geostatistical Wizard to produce a prediction surface map. The prediction map was then converted to raster format with the Geospatial Analyst *Layer to Grid* tool. Next, the raster images were extracted by mask to the shape of the basin polygon. The Raster Calculator was used to multiply the extracted, interpolated raster by its cell resolution. The output raster of the calculator and polygon of the basin was input into the *Zonal Statistics as Table* tool, outputting the volume of the multiplied raster in cubic meters. The conversions to wet sediment mass, dry sediment mass and dry

sediment volume are reported in Appendix E of Joyner (2016).

A prediction standard error surface map was also generated in the Geostatistical Wizard to measure the statistical accuracy of the prediction surface map. It is important to note that the standard error only reflects data locations, not data values. The prediction standard error surface map was used to produce the error estimate for the megaturbidite volume based upon the number of pixels in each interval of the prediction standard error surface range. First, the prediction standard error surface map was input as the conditional raster in the *Con* tool using an expression statement where VALUE <= 0.1. The input true constant value is 1 and the input false constant value is 0 such that the output raster has values of 1 where the pixels are <= 0.1. This was completed for each of the following ranges: 0-0.1, 0.1-0.2, 0.2-0.3, and 0.3-0.4. The number of pixels for each range is identified in the symbology heading of the *Con* output raster properties. The number of pixels for each range is multiplied by the prediction standard error raster cell resolution and the midpoint of the range to produce an overall volume estimate error, which is reported in Appendix F of Joyner (2016).

Displacement Wave Height Estimation

The displacement wave height estimates were derived following Evers and Hager (2016) whose empirical equation predicts displacement wave heights generated by rapid subaerial landslides impacting deep water bodies. The results have an associated estimated error of ± 30%. The empirical equation was derived by comparing wave heights generated by the scaled-down model of subaerial landslides to measurements predicted from the equation. The Evers and Hager (2016) equation was derived by combining parts of the empirical equations of displacement wave propagation by Heller et al. (2009) and Heller and Spinneken (2015).

Heller et al. (2009) equations:

$$F = \frac{V_s}{(gh)^{\frac{1}{2}}}$$

$$S = \frac{s}{h}$$

$$M = \frac{m_s}{p_w b h^2}$$

$$P = F^{0.5}\,2M^{0.25}\{\cos([6/7]\alpha)\}^{0.5}$$

Heller and Spinneken (2015) equation:

$$f_\gamma = \cos^{2\{1+\exp[-0.2(r/h)]\}}(2\gamma/3)$$

Evers and Hager (2016) equation:

$$\frac{H}{h} = 2P\left(\frac{r}{h}\right)^{-1} f_\gamma$$

The equations are dependent upon many fixed parameters, most of which were calculated in ArcGIS (Tables 2 and 3). The slide velocity is assumed to be 45 m/s. This estimate is based upon the 60 m/s velocity of a similar slide in Chehalis Lake, British Columbia whose vertical fall was greater than the Sledgehammer Point rockslide (Roberts et al. 2013). The propagation distance, propagation angle, and still water depth of each scenario was calculated in ArcGIS. The wave propagation distance (r) traveled by the wave is assumed to be in the shape of a straight line from the point where the rockslide enters the water to the scenario location. The propagation distance is the point just before the flat basin bottom starts to transition to the steep-sided lake margin. Due to the variability and uniqueness of lakes, wave heights on the opposite-shore slope cannot be calculated without numerical models; therefore the empirically derived equation can only be estimated for wave heights in the deep basin prior to breaking against the shoreline. The still water depths of the "opposite shore" and "Nature Bridge" scenarios are assumed to be 100 m. This "midpoint" depth was picked because the present day depths are 60-70 m where the subaqueous portion of the Sledgehammer Point rockslide is deposited and the pre-rockslide surface was most likely not deeper than 140 m (maximum depth of the north basin) (Fig 4).

Table 2. Dependent parameters of the Evers and Hager (2016) displacement wave height equation.

Parameter	Symbol	Dependent variables
Slide velocity	V_s	45 m/s
Gravitational acceleration	g	9.81 m/s^2
Slide mass	m_s	1.9 x 10^{10} kg
Water density	ρ_w	1000 kg/m^3
Slide thickness	s	55 m
Slide impact angle	α	45°
Slide width	b	820 m

Table 3. Independent parameters of the Evers and Hager (2016) displacement wave height equation.

Scenario Name	Propagation Distance (r)	Propagation Angle (γ)	Still water depth (h)
Log Cabin Resort	2624 m	+50º	140 m
Opposite Shore	1070 m	0º	100 m
Nature Bridge	950 m	-50º	100 m
U.S. Highway 101	6182 m	-40º	170 m

Results & Discussion

Lake Sediments

The cores sampled a sedimentary record that is up to 8,500 yr in length (Table 4; Fig. 8). Sedimentary deposits in the cores include both material that accumulated relatively slowly, representing "background" or everyday sedimentation, and discrete layers that accumulated during episodic events. Background material in the cores is predominantly composed of faintly laminated to massive light brown to gray diatomaceous silt and does not appear to record seasonal variations in sediment discharge or productivity (i.e., they are not varved) and represent every day or "background" sediment accumulation at an average rate of 0.6-0.8 mm yr^{-1} (Pollen, 2016). These sediments most likely originate from settling in the water column of fine-grained stream and tributary-derived clastic particles mainly originating from Barnes Creek, by far the largest tributary to the lake. Interstratified with these fine sediments are coarser, graded layers that contain a remarkable record of episodic lake disturbance. Two main types of event layers (EL1 & EL2) were distinguished from the background lake sediment using the magnetic susceptibility and density profiles of the cores as well as visual analysis (e.g., Figs. 8, 9).

Table 4. Radiocarbon geochronology of Lake Crescent sediment cores.

Lab ID	Core	Core Segment	Depth in core segment (cm)	$\delta^{13}C$ (‰)	fraction Modern (pMC)	^{14}C age (ybp)	2σ cal ^{14}C age (ybp) and probability	Median cal ^{14}C age (ybp)	error bars	Event Layer	NOTE - 1
D-AMS 015265	4A	1K-1	76.5-78	-19.2	51.2 ± 0.2	2114 ± 29	2290 - 2270 0.007) 2160 - 1990 (0.947)	2090	150	EL1[A]	
D-AMS 015277	7A	1K-1	85-86	-22.2	74.1 ± 0.26	2408 ± 28	2690 - 2630 (0.089) 2610 - 2590 (0.018) 2500 - 2350 (0.847)	2450	170	EL1[A]	The central age for Megaturbidite A (EL1) of 3140 ± 95 was determined fom the calibrated radiocarbon ages to the left. The event layer age must be younger than the oldest age for material derived from stratigraphically above the event layer (assuming no in-built age; which is perhaps not a valid). So, EL1 must be as old or older than 3045 cal yr BP (D-AMS 013818; 2940 + 105 cal ybp) and younger than the oldest plausible age for material collected from within the EL1 deposit at 3230 cal ybp (D-AMS 013811; 3130 + 100 cal ybp).
D-AMS 015275	6A	1K-3	81-82	-20.9	72.79 ± .023	2551 ± 25	2750 - 2690 (0.660) 2640 - 2610 (0.082) 2600 - 2500 (0.215)	2680	125	EL1[A]	
D-AMS 013818	4A	1K-2	85.5-86.5	-21.8	70.26 ± 0.3	2835 ± 34	3060 - 2850 (0.954)	2940	105	EL1[A]	
D-AMS 013812	9A	1K-2	41-50	-26.3	70.87 ± 0.25	2766 ± 28	2950 - 2780 (0.954)	2860	85	EL1[B]	
D-AMS 013814	6A	1K-4	140-141	-22.3	69.44 ± 0.31	2930 ±36	3180 - 2960 (0.954)	3080	110	EL1[B]	
D-AMS 013809	2C	1K-1	100-105	-35.4	69.26 ± 0.25	2951 ± 29	3210 - 3000 (0.954)	3110	105	EL1[B]	
D-AMS 013811	7A	1K-4	2-6	-26.2	69.11 ± 0.23	2968 ± 27	3230 - 3030 (0.954)	3130	100	EL1[B]	
WHAMS-129388	8A	1K-4	72-74	*	64.95 ± 0.14[$]	3510 ± 15	3840 - 3710 (0.954)	3780	65	EL2[A]	The central age for Megaturbidite B (EL2) of 4,000 ± 90 cal ybp was determined from the fact that MTB must be younger than D-AMS 013819 minimum age of 4090 cal ybp; Therefore range for D-AMS 012813 must be 4090-3910, or 4,000 ± 90, because maximum limiting age of 4,090 from the sample collected beneath the MTB layer in core 8A
D-AMS 013813	9A	1K-2	98-100	-26.5	63.3 ± 0.21	3673 ± 27	4090 - 3910 (0.954)	4010	90	EL2[B]	
WHAM-129389	8A	1K-6	115-116	*	62.14 ± 0.14[$]	3820 ± 20	4290 - 4140 (0.954)	4200	50	EL2[C]	
D-AMS 013819	4A	1K-3	26-26.5	-34.8	62.1 ± 0.21	3827 ± 27	4410 - 4320 (0.067) 4300 - 4141 (0.869) 4120 - 4090 (0.018)	4230	160	EL2[C]	
WHAMS-130043	2A	1K-5	71-72	*	58.86 ± 0.21[$]	4260 ± 30	4870 - 4810 (88.4%) 4760 - 4710 (7.0%)	4830	80	EL3[B]	MTC (EL3) is constrained by minimum age of WHAMS-130043 (4710 cal ybp) and minimum of WHAMS-129391 that was collected from beneath MTC deposit in core 8A, this its minimum age must be a limiting maximum for the event. The two samples WHAMS-130045 & 130046 were collected from within the MTC event layer, but they are older than sample WHAMS-129391; therefore they must have in-built ages associated with the material that we dated, perhaps resuspension of deposits already on the lake floor at the time of the MTC event
D-AMS 013820	4A	1K-3	133-134	-38.5	57.88 ± 0.24	4392 ± 33	5210 - 5200 (0.005) 5050 - 4860 (0.949)	4960	175	EL3[B]	
WHAMS-130046	2A	1K-1	123-126	*	57.38 ± 0.20[$]	4460 ± 30	5290 - 4860 (0.954)	5070	215	EL3[B]	
WHAMS-130045	2C	1K-1	128-130	*	57.03 ± 0.17[$]	4510 ± 25	5300 - 5210 (0.317) 5200 - 5040 (0.637)	5170	130	EL3[B]	
WHAM-129391	8A	1K-7	38-41	*	57.53 ± 0.13[$]	4440 ± 20	5280 - 5160 (0.256) 5130 - 5100 (0.017) 5070-4960 (0.682)	5070	160	EL3[C]	
D-AMS 013817	2C	1K-5	45-46	-27.3	46.17 ± 0.19	6208 ± 33	7250 - 7000 (0.954)	7100	125	EL4[B]	MTD (EL4) is constrained by the minimum age of D-AMS 013817 (7,000 cal ybp) and the maximum age of D-AMS 015286 (7,270 cal ybp).
WHAMS-130044	2A	1K-5	119-120	*	45.99 ± 0.15[$]	6240 ± 25	7260 - 7150 (0.815) 7120 - 7020 (0.140)	7180	120	EL4[B]	
D-AMS 015268	4A	1K-4	114-124	-21.1	45.72 ± 0.17	6287 ± 30	7270 - 7160 (0.954)	7220	55	EL4[B]	
	4A	1K-5	119-120				7680 - 7590	7630	45	EL4[D]	Median age of Mazama Ash (Egan et al., 2015)

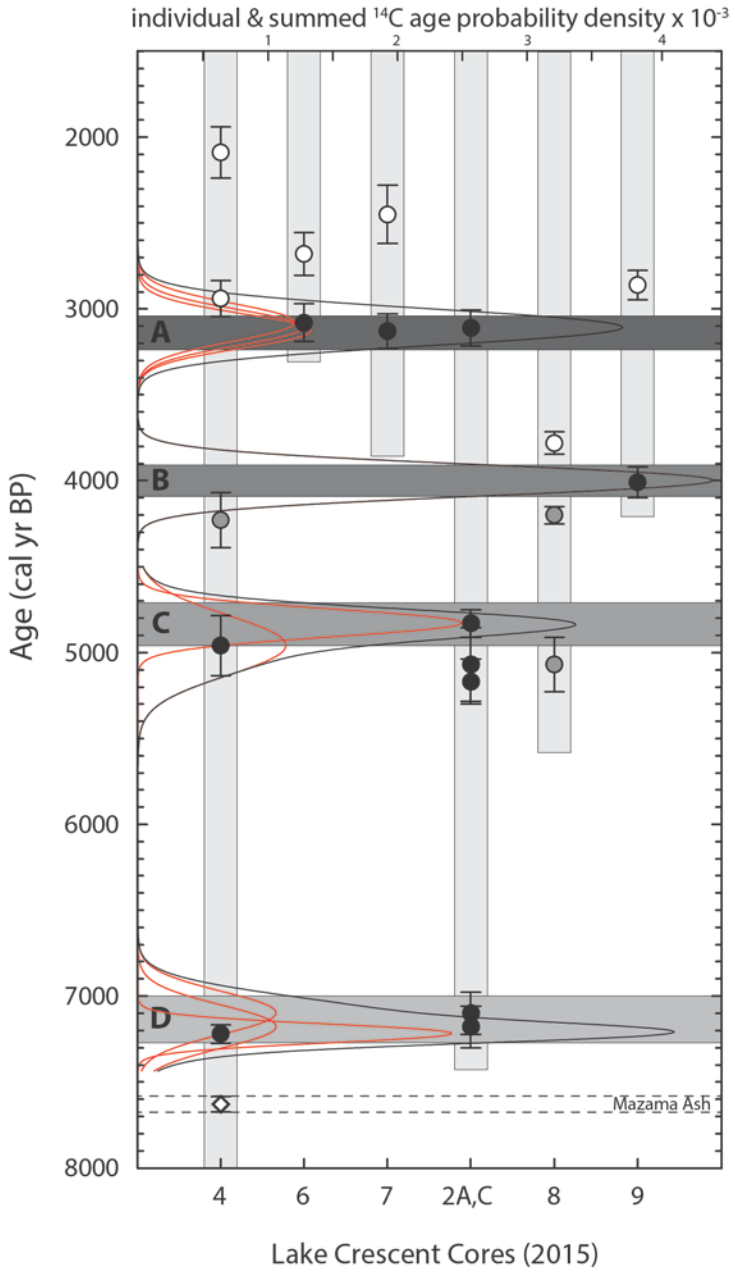

Figure 8. Radiocarbon-based chronology for piston cores recovered from Lake Crescent in 2015, with gray bars showing correlation of megaturbidite layers (from the youngest to oldest) A, B, C, and D, between the cores. Solid symbols show the calibrated 2-sigma age range of samples from within the layers themselves, while white and gray symbols are for samples above and below the layers, respectively. The unfilled diamond shows the published age range of the Mazama tephra, which is approximately 2 cm thick in core 4A. The individual (red lines) and summed (black line) age probability distributions of the calibrated radiocarbon dates are overlain on the megaturbidite age determinations.

Event Layer 1 Deposits - Megaturbidites

The first type of sedimentary event layer deposit (EL1) distinguished from the background sediment range in thickness from 12 cm in core 4A to an average of ~170 cm in cores obtained from the deep middle portions of both lake basins. In total, four 1 to 2 m thick, normally graded EL1 layers were sampled and were designated A, B, C, and D, from youngest to oldest (Fig. 8). Following Bouma (1987), we term the layers *megaturbidites* (see also Schnellmann et al., 2005; Hilbe and Anselmetti, 2014; Moernaut et al., 2014). Figure 9 shows a photo of the uppermost of these layers (layer A) in core 2, along with particle size and magnetic susceptibility data. Sitting on a basal scour surface, the layer comprises approximately 40 cm of laminated, normally graded, coarse to medium sand overlain by a 100-cm-thick interval of homogeneous silt with abundant, disseminated plant debris and evidence for soft-sediment deformation. The silt bed is in turn overlain by a 10-cm-thick layer of fine clay, and a few centimeter-thick sequences of interstratified laminae of fine basaltic sand and green chloritic clay. As exhibited in Figure 9, the coarse basal sand units are characterized by high magnetic susceptibility while the clay caps are characterized by low values. Fairly consistent magnetic susceptibility values characterize the central, silt layer (Fig.9).

Radiocarbon dates from plant debris incorporated into megaturbidite A in multiple cores (Figs. 8, 10) indicate emplacement at 3140 ± 95 (3045-3235) cal yr BP (Table 4). The homogeneous silt bed corresponds to the uppermost acoustically transparent unit (unit A) first observed in seismic reflection profiles from both the northern and southern basins of Lake Crescent (Fig. 5). Based on these profiles, the layer has a wet volume of approximately 4.8 x 10^6 m^3 (Joyner, 2016). The layer is coarsest and thickest in the northern basin of Lake Crescent, where it is locally 2 m thick (Figs. 11). It thins towards the margins of the lake, and in the western most sub-basin of the southern basin it is only 10 cm thick (core 4; Figs. 4, 11, 12). Based on its pattern of thickness and maximum particle size, as well as its absence from depressions atop the subaqueous landslide debris between the north and south deep basins of the lake (Fig. 12), the layer can be attributed to the Sledgehammer Point rockslide, which initiated 700 m above the lake and descended into water that is estimated to have been 100 ± 40 m deep (Fig. 4; 14). The slide occurred in the Crescent Formation and deposited an

estimated volume 7.2 ± 1.8 x 10^6 m^3 of basaltic rock into the lake, while the slide mass is estimated to be 11.9 x 10^6 m^3 based upon landslide area-to-volume scaling relationship of Larsen et al. (2010). Notably, the sand at the base of the megaturbidite is moderately well rounded and is of mixed basalt and sedimentary provenance, indicating that it was not derived directly from the slide material, but from remobilization of material already in the lake (Joyner, 2016).

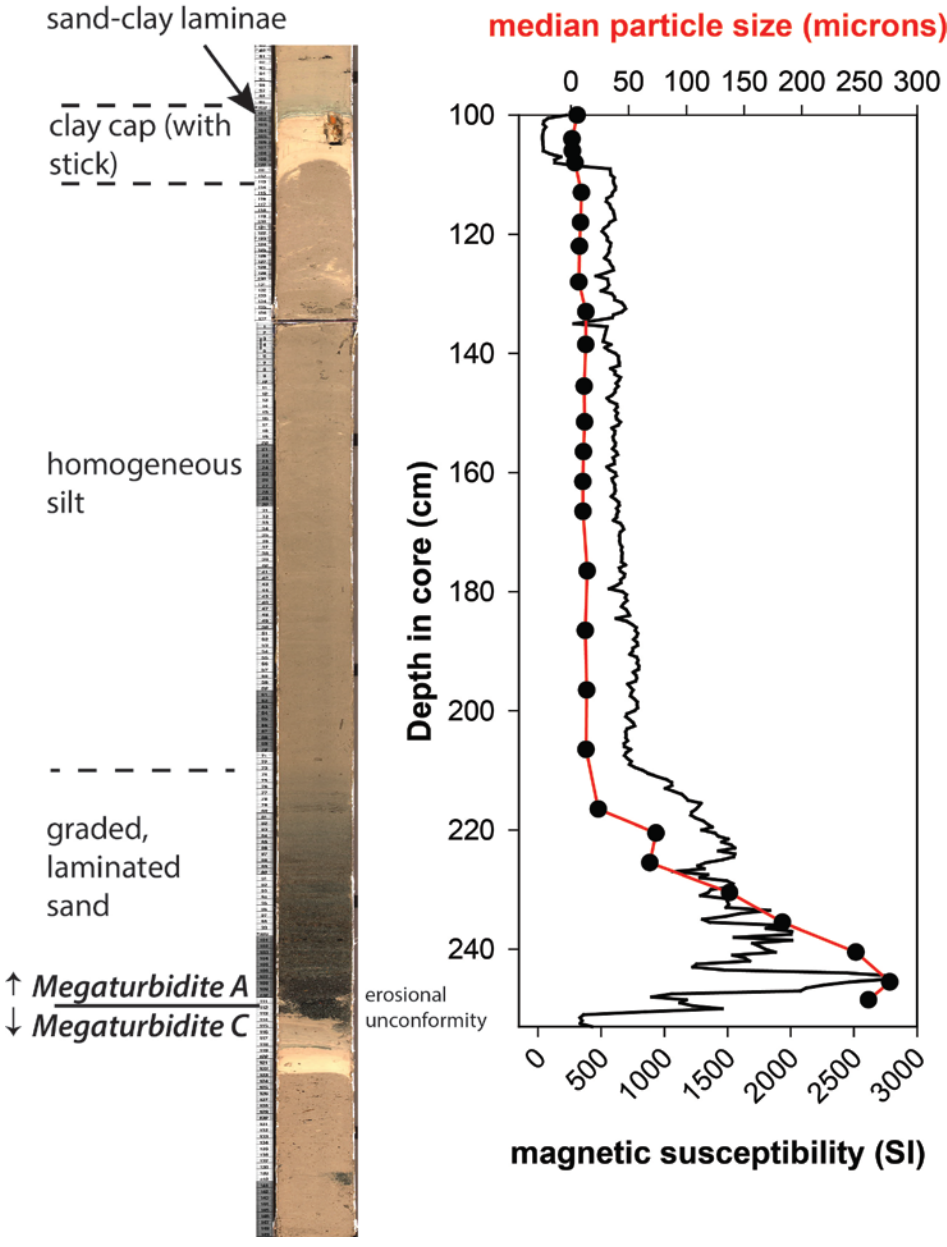

Figure 9. Photos of a portion of core 2C, showing megaturbidite A (dated at 3140 ± 95 cal yr BP) sitting with erosional contact on megaturbidte C (dated at 4835 ± 125 cal yr BP). Also shown are magnetic susceptibility and laser particle size measurements for megaturbidite A. Note the scale to the left of the core photos, where gray bars indicate 10 cm. At core site 2C, megaturbidite A is ~ 150 cm thick (see Figs. 4 and 5 for spatial reference).

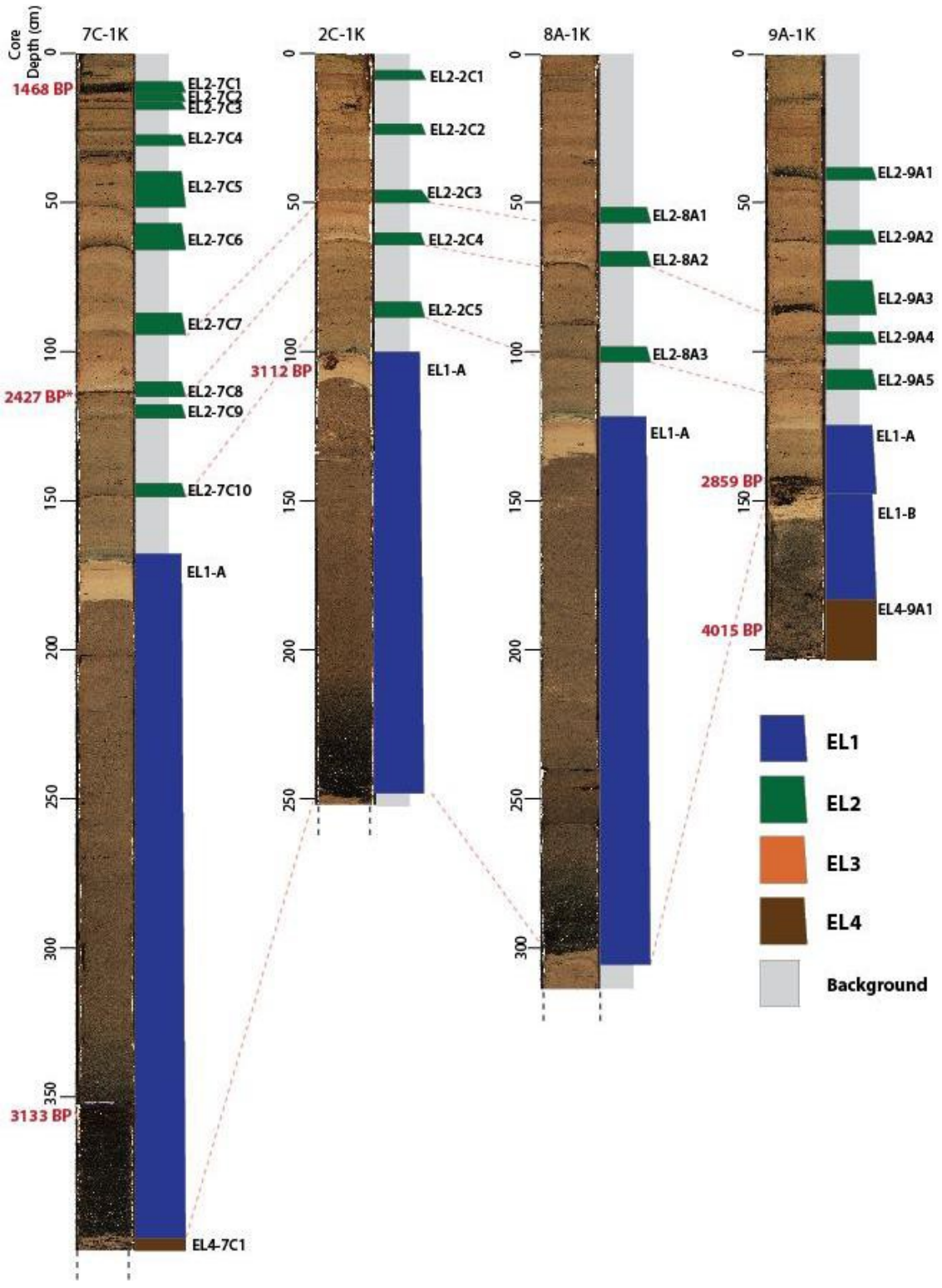

Figure 10. Event layers correlated across the northern basin of Lake Crescent. Event layers are identified in the core images and their corresponding stratigraphic columns and correlated where possible. Dashed red lines correlate layers from the base of the deposit. Event layers are

identified by their respective type, core ID, and order from top of each core; for example, EL2-4A1 is a type EL2 sedimentary deposit in core 4A-1K and is the uppermost EL2 unit recognized in the core. See Appendix 3 of Pollen (2016) for a description of each event layer present in the sediment record.

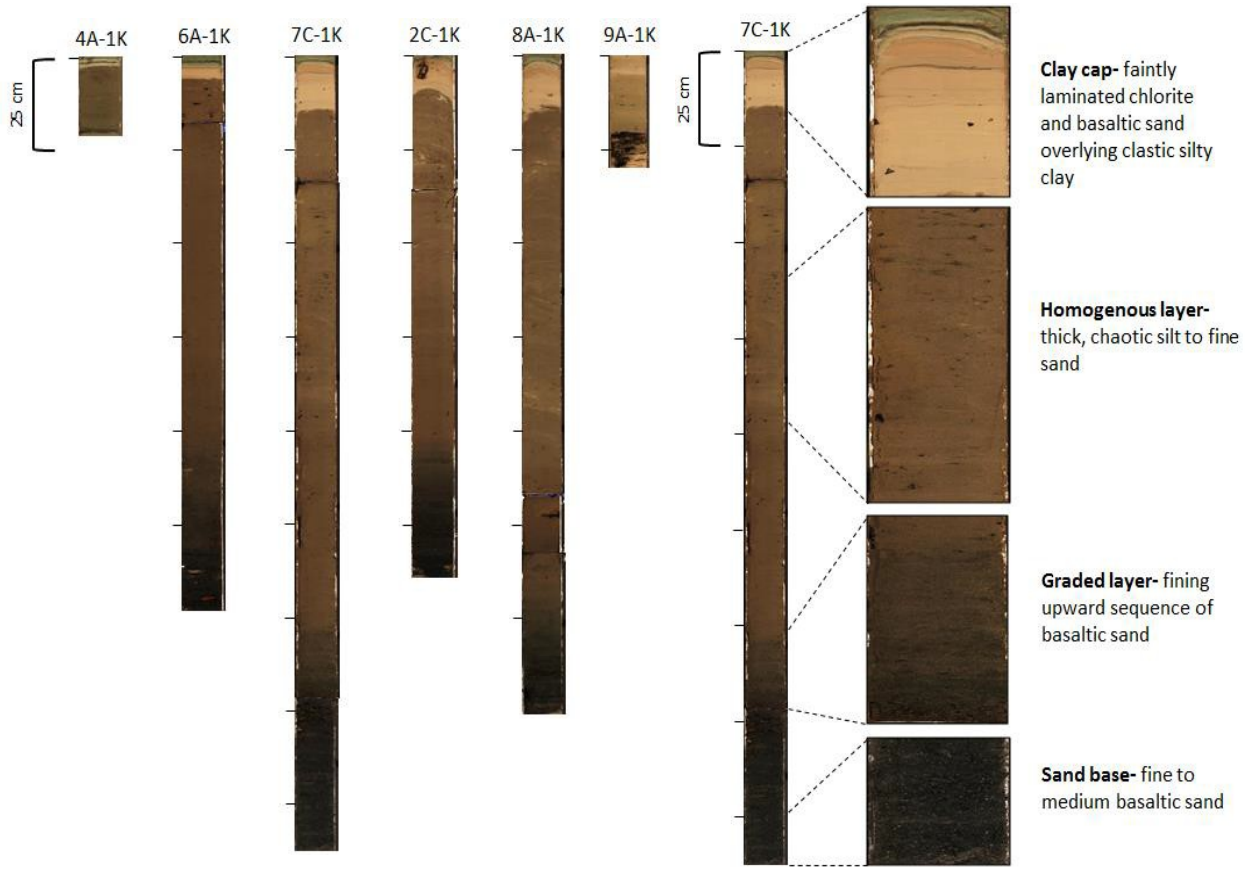

Figure 11. Six core images of the EL1-A layer arranged from west to east across the lake. The EL1-A deposit consists of an erosively based, normally graded basaltic sand layer overlain in turn by massive, homogenous silt with dispersed plant debris and a clay cap interstratified with chloritic clay and basaltic sand laminations except in core 9A-1K, which lacks the laminations.

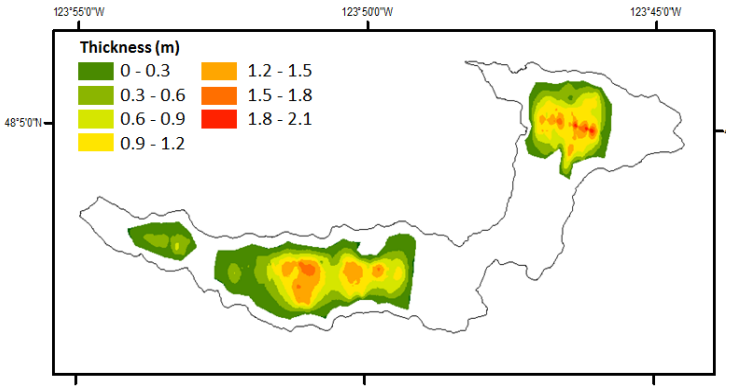

Figure 12. Isopach map of megaturbidite A based on CHIRP seismic reflection date (from Joyner, 2016).

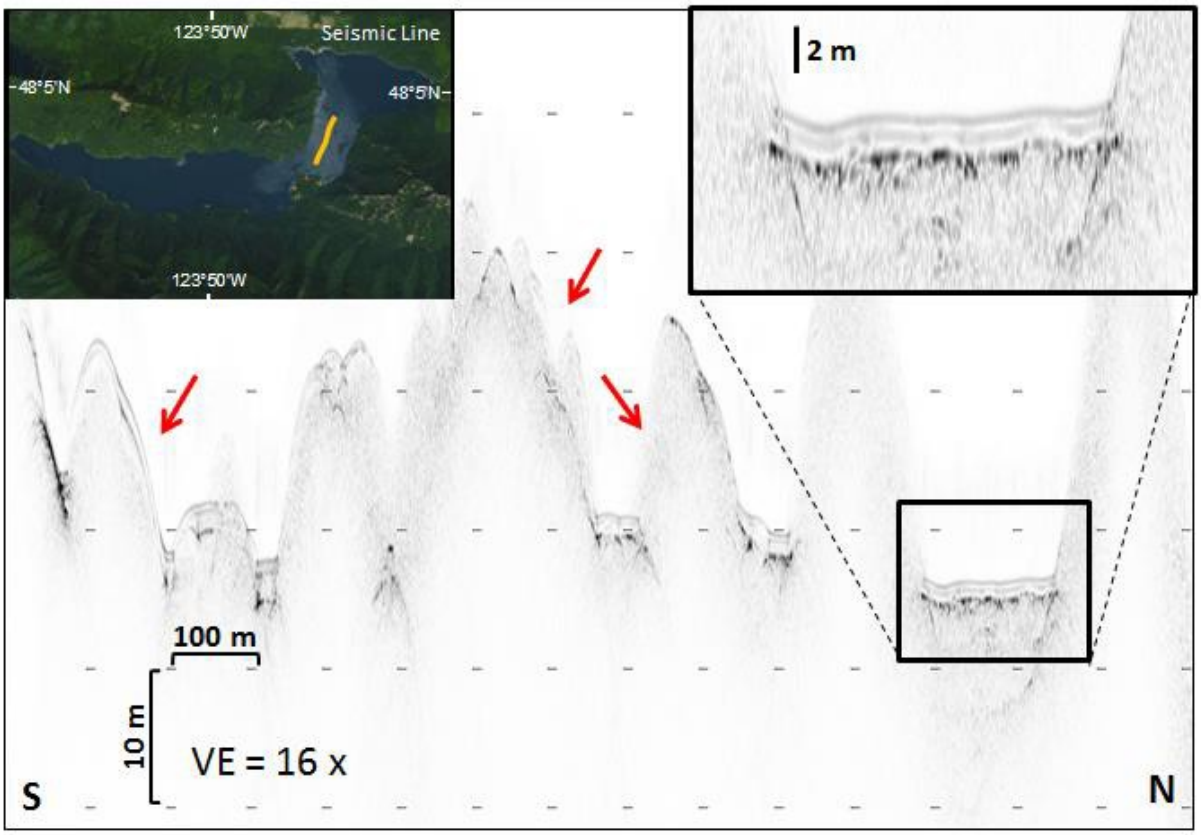

Figure 13. Seismic line from the central channel between the north and south basins (see map inset) across a portion of the Sledgehammer Point rock slide deposit. The red arrows point to the parts of the tallest subaqueous rockslide deposits. The inset image of the small intra-deposit depressions (see map inset) shows the presence of about 1.5 to 2 m of *Seismic Facies A*, but no *Seismic Facies B* deposit (megaturbidite) deposits. This observation suggests that the Sledgehammer Point landslide is only a few thousand years old. The vertical exaggeration is 16x, and the top of the tallest mounds on the landslide are in 60 m of water in this image.

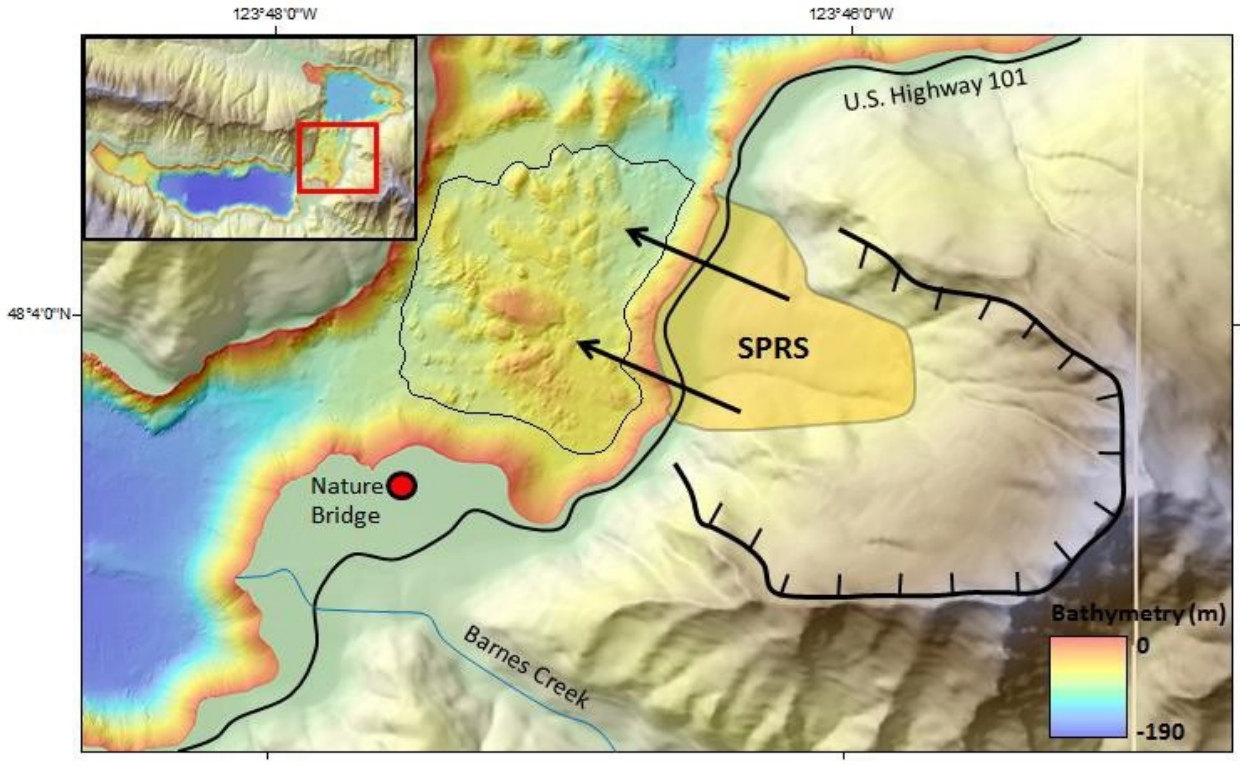

Figure 14. The onshore Sledgehammer Point rockslide (SPRS) is shaded yellow and the subaqueous portion is outlined in black. The hachures point down scarp. The arrows indicate the direction of movement. Bathymetric grid has a resolution of 3 m, while the terrestrial DEM has a 10 m resolution (USGS, 2001).

Relationship between Mass Wasting and Megaturbidite Event Layers

Upon entering the lake, the Sledgehammer Point rockslide would have triggered a displacement wave (lake-tsunami), likely similar to the modern analog event that occurred in March, 2007 at Chehalis Lake, British Columbia, Canada (Roberts et al., 2013). Evers and Hager (2016) investigated displacement waves triggered by landslide events into deep water bodies and derived empirical equations to predict maximum deep-water displacement wave heights. Joyner (2016) applied the equations and arrived at estimates of deep-water wave height resulting from a Sledgehammer Point landslide scenario, such that directly in front of the landslide entry point, the opposite shore wave height would be 20 ± 6 m about 140 m offshore. Open water wave heights systematically decrease with distance and back-azimuth angle to the location of landslide entry (Fig 15). Using the global relationship of observed maximum displacement wave run-up height as a function of landslide volume (Clarke et al., 2015), we

estimate that the opposite-shore deep-water wave would transition to a maximum breaking wave run-up height of 85 ± 17 m above modern lake level (Figs. 4, 15), and that the height of the wave would decrease as it propagated along the shoreline in a complicated and non-linear fashion away from the point of landslide entry.

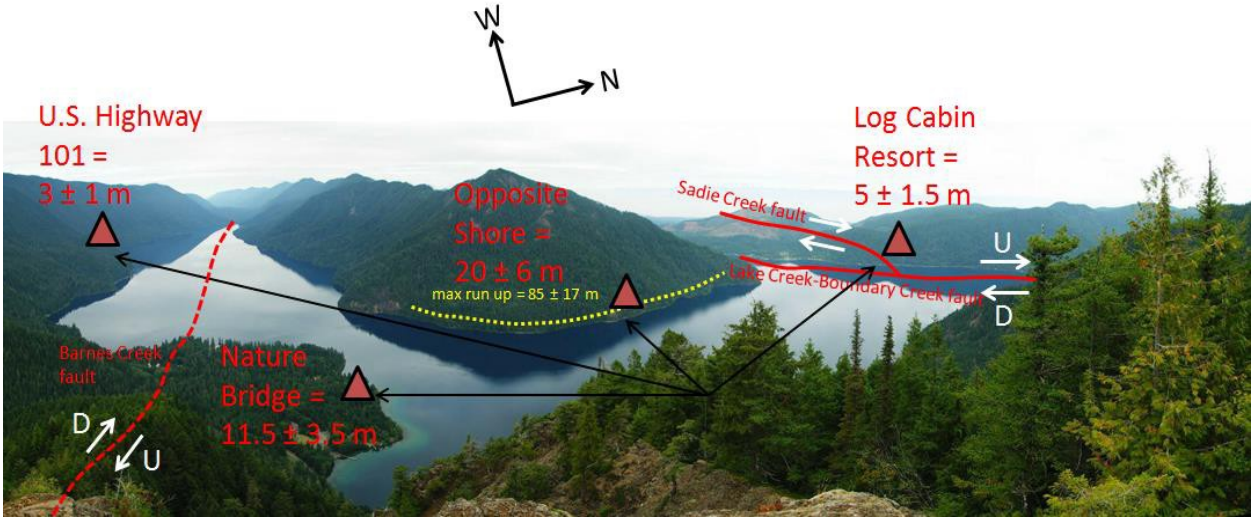

Figure 15. Photograph from Mt. Storm King looking west-northwest across Lake Crescent. The straight line propagation rays (black arrows) of the displacement wave from the c. 3100 cal yr BP Sledgehammer Point landslide where it entered the lake to the shore at the four model locations (red triangles). Wave heights at each location are reported in red. The maximum wave run up on the opposite shore is outlined in yellow. The Sadie Creek, Lake Creek-Boundary Creek, and Barnes Creek faults are drawn in red. Right lateral motion is indicated by the white arrows. Vertical motion is indicated by U (up) and D (down).

As the wave train travelled through the lake, it likely entrained sand from shallow subaqueous environments, which was then transported as a concentrated density flow along the lake bottom. In the process, the existing lake floor was scoured, and fine particles were suspended into the water column. After the initial wave, periodic oscillations (seiche) likely aided in the distribution of the suspended material throughout the lake, and ultimately resulted in the repeated (multiple) grading observed at the base of the megaturbidite and the formation of the thick, homogenous silt layer (e.g., Schnellmann et al. 2002; Beck, 2009; Howarth et al 2012; Hilbe and Anselmetti, 2014). Days to weeks after the rockslide-displacement wave event, the finest suspended particles would have settled to the lake floor to form the clay layer that caps each of the megaturbidites. We interpret the series of basaltic sand and chloritic clay

laminae overlying the clay cap to record transport and settling of sediment derived from the rockslide scar or from disturbed stream catchments surrounding the lake in the months to years following the triggering event (Figs. 16).

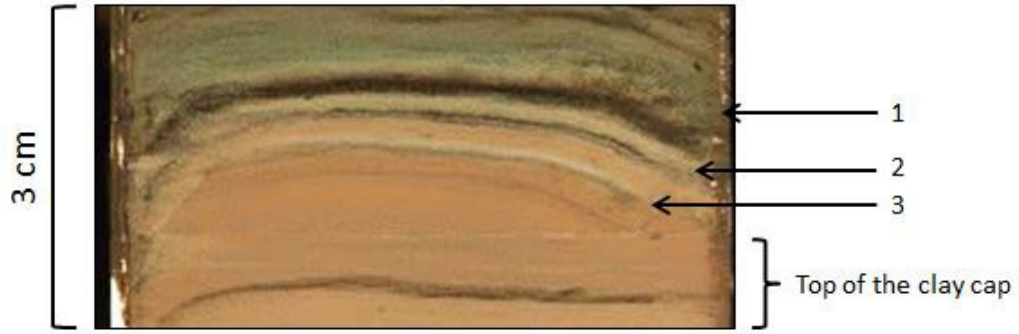

Figure 16. Three sequences of chloritic and basaltic laminations (1-3) superimposed on the clay cap of the EL1-A deposit in core 7C-1K. The interstratified laminations are only found at the tops of megaturbidites which are interpreted to be the mobilization of sediment from the subaerial portion of the exposed rockslide scarp during precipitation events in the years after the mass wasting event, or from stream response to mass wasting in tributary basins (e.g. Barnes Creek) in the months to years after the triggering earthquake.

The three earlier megaturbidites sampled in our study share characteristics that are remarkably similar to those of megaturbidite A. Megaturbidite B is patchily preserved in the northern basin, where it was apparently partially eroded away during the subsequent megaturbidite A event (Figs. 5; 17). It is found, however, near the eastern limit of the lake in core 9A atop landslide debris (gravel and interspersed plant debris) attributed to the Lake Sutherland rock slide complex (Figs. 4; 16, 18). Pringle et al. (2010) and Wegmann et al. (2014b) estimated that the mass failures that isolated Lake Crescent from Lake Sutherland and led to a lake level rise of 25 m, occurred sometime soon after 4,340 ± 50 cal yr BP based on radiocarbon dated growth rings in a drowned tree rooted in 18 m water depth at the west end of Lake Crescent's south basin. The age of megaturbidite B (4000 ± 90 cal yr BP) is consistent with this earlier estimate (Fig. 8).

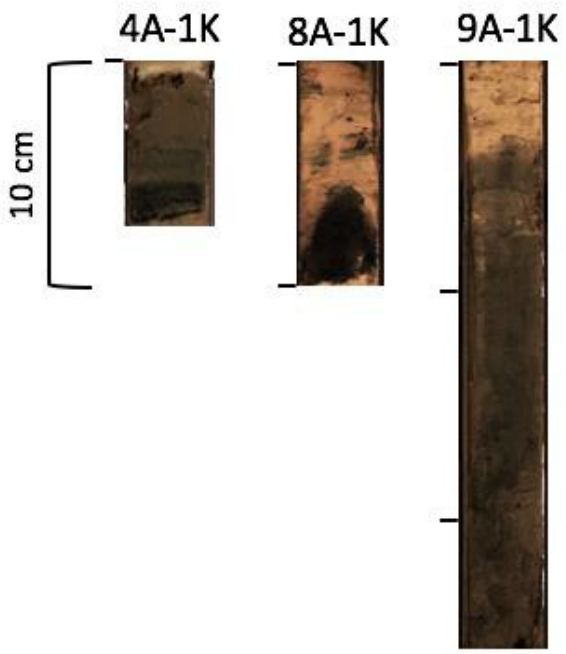

Figure 17. EL1-B megaturbidite core photographs from Lake Crescent arranged from west to east.

Figure 18. View to the northeast (towards Cascade Range) from Pyramid Peak (opposite shore to Mt. Storm King) showing the coalescing rockslides that separated Lake Crescent from Lake Sutherland c. 4,000-5,000 cal yr BP. Photo by Jeff Taylor, downloaded on September 20, 2016 from: https://en.wikipedia.org/wiki/Lake_Crescent#/media/File:Lake_Crescent_from_Pyramid_Pea k.JPG.

Megaturbidite C is dated at 4835 ± 125 (4960-4710) cal yr BP (Fig. 8; Table 4). It was recovered in core 4 from the western portion of the south basin and cores 2, 3, 7 and 8 from the north basin (Fig. 19). The Mount Storm King rockslide, located across the valley from the Lake Sutherland rock slide, is a potential trigger for its deposition into the ancestral portion of Lake Crescent that was closed off by the Megaturbidite B event c. 4,000 cal yr BP (Figs. 4, 18). Charcoal collected from sediments that accumulated within a closed depression on the surface of the rockslide provides a corroborating age of 5,150 (5,290-4970) cal yr BP (Joyner, 2016). The location of the rockslide that triggered the formation of megaturbidite D, which was deposited 7135 ± 135 (7000-7270) cal yr BP and recovered in one core from both the north and south basin, is less certain (Fig. 20). It is evident from the high-resolution multibeam bathymetry data from Lake Crescent, however, that there are other as of yet undated mass wasting deposits that exist along the margins of Lake Crescent (Fig. 4).

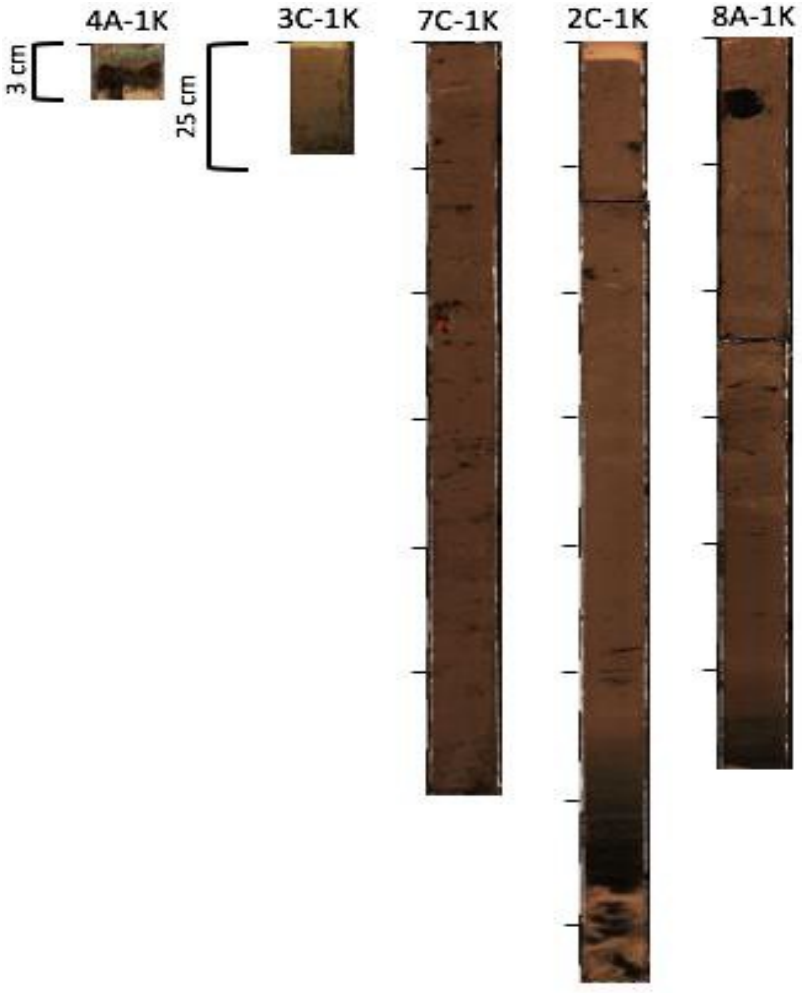

Figure 19. Five core images of the EL1-C megaturbidite layer arranged from west to east across Lake Crescent.

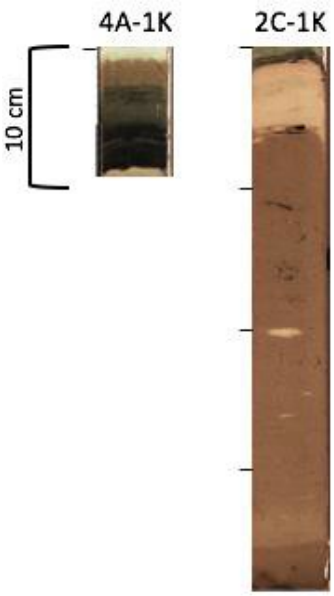

Figure 20. Two core images of EL1-D megaturbidite layer arranged from west to east across Lake Crescent. The deposit in core 2C was only partially recovered.

Earthquake Triggering of Megaturbidite Event Layers

Subaerial and subaqueous mass wasting events, both seismogenic and unrelated to earthquakes, are known to have been triggered displacement waves in fjords and lakes around the world, including in Lituya Bay, Alaska, Tafjord Fjord, Norway, and Lake Chehalis, Canada (Fritz et al., 2009; Sassa and Canuti, 2009; Roberts et al., 2013). The largest known displacement wave, with 524 m of run-up, is the 1958 Latuya Bay event, which occurred when an M_w 8.3 earthquake along the Fairweather Fault triggered a major subaerial landslide (Fritz et al., 2009). In Lake Crescent, seismic reflection data clearly demonstrate that the most recent megaturbidite (EL1-A) is undeformed where it is deposited above the trace of the Lake Creek – Boundary Creek and Sadie Creek faults. Our seismic reflection data are interpreted as recording the progressive deformation of each of the deeper and older seismically-transparent units identified in the cores as megaturbidite layers (EL1-B – D). This observation is consistent with slip on both fault strands beneath the northern basin of Lake Crescent (Fig. 5), and for this reason, the temporal correlation between earthquakes on the LCBCFZ, subaerial mass wasting into Lake Crescent and the generation of displacement and seiche waves necessary for the formation of the observed and dated megaturbidite layers EL1-A through EL1-D. Recent fault trench records (Nelson et al., 2007, in press; Figs. 2 & 21), provide corroborating evidence for a

rupture of the fault to the east of the lake ca. 3000 cal yr BP and one or two between 5-8 cal yr BP that could correlated to the megaturbidite C or D events. Interestingly, the ca. 4000 cal yr BP (megaturbidite B) Lake Crescent event was not recognized in the fault trench records, and a 1300 cal yr BP event recognized by Nelson et al. (2007; in press) did not affect the lake (Fig. 21). Although there are several possible explanations for this discrepancy, one is that the LCBC-Sadie Creek fault system is segmented and does not always rupture along its entire length. If true, segmented behavior would have important implications for estimating the intensity of past and future earthquakes. Paleoseismic trenching surface rupture features recently recognized along the Sadie Creek fault to the west of Lake Crescent (Joyner, 2016; Nelson et al., in press) will be important to testing for (1) segmented, or partial rupture behavior along the LCBCFZ. For example, the Lake Crescent megaturbidite record predicts that the Sadie Creek fault did not rupture c. 1,300 years ago, as did the LCBCF to the east of Port Angeles (Nelson et al., 2007; in press). If future paleoseismic trenching indicates that the Sadie Creek fault likely did rupture c. 1,300 cal yr BP than this might indicate that the earthquake did not generate a large enough landslide into Lake Crescent for the formation of a 1 to 2 m thick megaturbidite layer. In such a scenario, the EL1-type megaturbidite record would then need to be considered as a partial account of the LCBCFZ earthquakes at Lake Crescent.

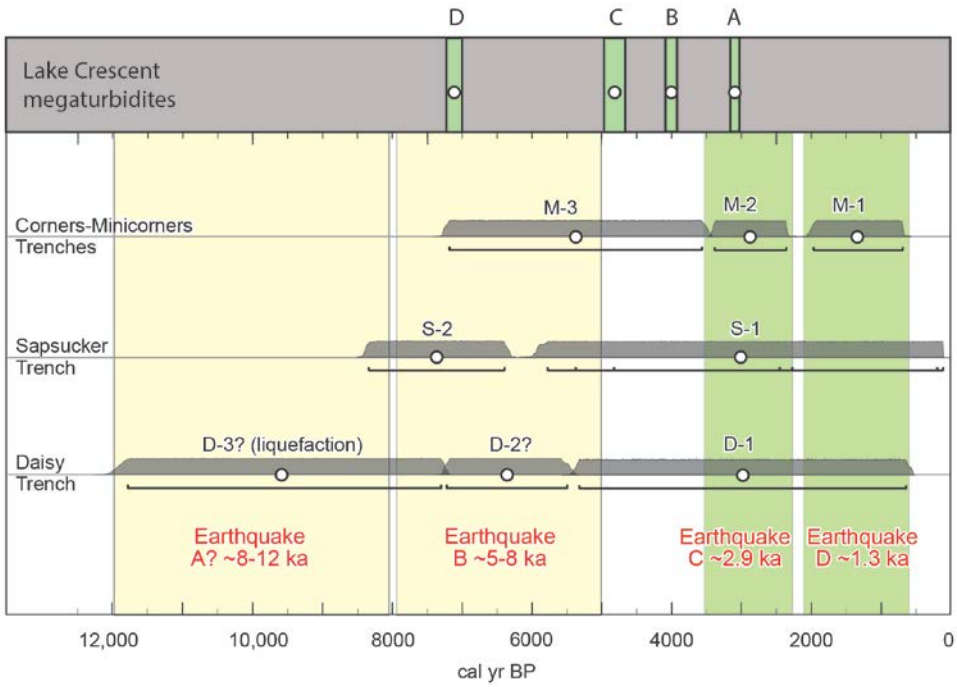

Figure 21. Comparison between the ages of earthquake-triggered megaturbidites in Lake Crescent and the earthquake-age probabilities compiled by Nelson et al. (2007; in press) based on fault trenching along the LCBCF c. 30 km to the east of the lake. See Figure 2 for trench locations.

Additional Event Layer Deposits

A second common type of event layer present in the Lake Crescent stratigraphy, EL2, comprise thinner (4-33 cm), normally graded layers of fine sand to clay. These layers have sharp and often erosive basal contacts, typically overlain by several centimeter thick (maximum 4 cm) basal layer consisting of massive to fining upward basaltic sand with rare laminations (Pollen, 2016). The basaltic sand is mixed with varying amounts of woody material, and then is topped by a unit of medium brown to dark gray silty sediment with fragments of wood interspersed (Fig. 10). Magnetic susceptibility values peak where basaltic sand is present and decrease or remain stable through the layer above indicating that the overlying silt is normally graded or homogeneous. A few of the EL2 deposits have a <5 cm thick layer of light colored, fine clayey material overlying the central silt unit. EL2 layers differ from EL1 deposits in that they are thinner and show considerable variation in composition, particle size, and sedimentary fabric across the lake basins (Joyner, 2016; Pollen, 2016). The layers are thicker (average ~14 cm) in the deepest portion of the southern basin and thinner in the elevated, and somewhat isolated, western depression of the southern basin and in the northern basin (average ~4.5 cm).

EL2 layers are interpreted to be turbidite deposits based on their sharp, erosive bases and normal grading (e.g. Bouma, 1987). Turbidites may have formed in Lake Crescent through several mechanisms, including earthquake triggered remobilization of sediment from the lake margin, or from episodic riverine flood events. In the southern basin, ten EL2 units can be correlated between cores 5 and 6, which are ~1 km apart in the center of the deepest part of the basin (Fig. 4). These correlated event layers range from 4 to 33 cm with an average thickness of ~14 cm. Using the area of the flat bottom of the southern basin (where EL2 layer thickness is inferred to be consistent) and assuming a porosity of 40%, it is estimated that between 5.6×10^5 to 4.6×10^6 (average 2×10^6) tons of sediment were deposited during a single EL2 forming event (Appendix 4 of Pollen, 2016). This converts to between 77 and 631 (average 268) years of average sediment yield represented by each EL2 deposit in the southern basin (Pollen, 2016). For the smaller northern basin, the average EL2 layer thickness is 4.5 cm, with a range of 3 to 12 cm. Using the aforementioned 40% porosity and the surface area of the flat bottom of the northern basin, the amount of sediment deposited instantaneously during a

single EL2 event ranges from 2.3 to 9.2 x 10^5 (average 4.5 x 10^5) tons which represents c. 600 to 2400 (average 895) years of sediment accumulation in the northern basin (Pollen, 2016). It cannot be discounted that at least some of the thinner layers may represent large hydrologic flood events (e.g. 100 year RI floods), but the thick layers that represent hundreds of years of sediment yield deposited fairly instantaneously most likely have a different origin, such as earthquake triggered remobilization of sediment perched on deltas and steep slopes around and within the lake.

Individual EL2 layers were correlated visually, accounting for their respective ages, and grouped into 19 Lake Crescent Turbidite layers (LCT), 11 of which were deposited since the EL1-A megaturbidite at about 3,100 cal yr BP (Table 3 of Pollen, 2016; Figs. 10, 22). These 19 LCT layers are tentatively assigned a seismic origin due, in part, to their substantial thickness that is representative of greater than 100 years of estimated annual suspended sediment yield. Several of the EL2 deposits may contain sediment from more than one source, which is indicative of a mechanism that triggered remobilization of material in multiple locations, such as an earthquake (e.g., Moernaut et al., 2014; Van Daele et al., 2015). Our interpretation of the EL2 layers is that they are primarily the sedimentary response to ground shaking

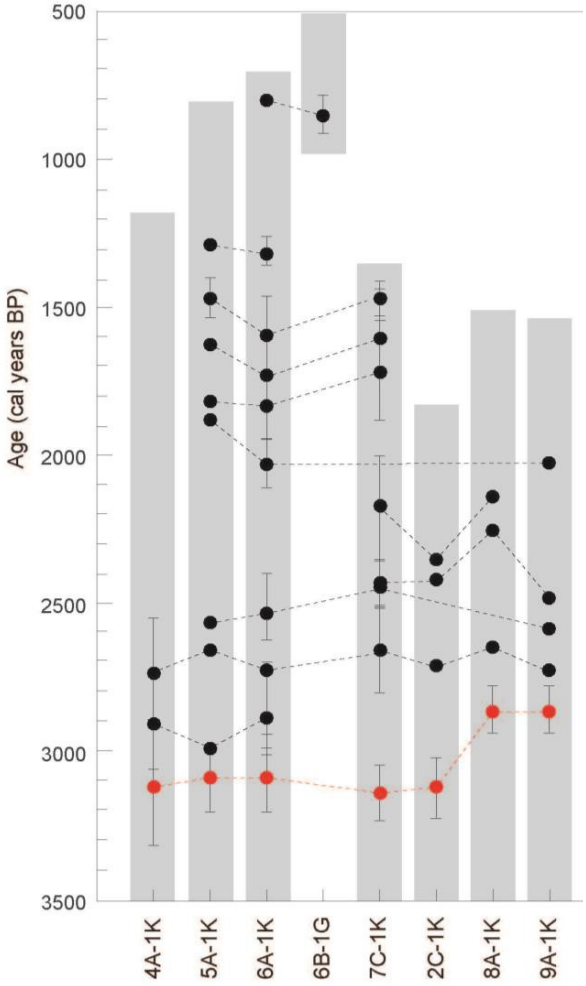

Figure 22. EL2 layers correlated (dashed black lines) above the first megaturbidite deposit (EL1-A) that is indicated by red symbology.

caused by regional earthquakes on faults other than the LCBCFZ, perhaps including the Cascadia megathrust and potentially other nearby active upper crustal faults (e.g. Morell et al., 2017); however additional research including more detailed geochronology is needed in order to test this hypothesis.

Conclusions

Improving estimates of the sizes, recurrence intervals, and effects of late Quaternary earthquakes in the Puget Sound region, and evaluating earthquake-induced ground failure potential near bodies of water where landslides may generate local tsunamis are two of the research priorities for the Pacific Northwest (PNA) region of the National Earthquake Hazards Reduction Program. Direct physical evidence exists for surface ground ruptures both beneath Lake Crescent as well as to the west and east of the lake for a distance of at least 56 km. For this NEHRP-funded research project, we acquired high-resolution multibeam bathymetric data and a suite of piston cores to determine that landslides entering Lake Crescent have produced four lake tsunami/seiche events during the past 8500 years, around 3100, 4000, 4900, and 7200 cal yr BP. When combined with seismic reflection data collected earlier, there is substantial evidence indicating that these events locally caused meters of erosion into the lakebed, and deposition of "megaturbidite" layers that are traceable over the entire 20 km^2 lake basin and exceed 1 m thickness over much of the deep lake floor. The c. 3100-yr BP megaturbidite deposit has an estimated volume of about 4.8 x 10^6 m^3. Preliminary modelling suggests that it was produced by an earthquake-triggered rockslide into the lake that would have generated a displacement wave (lake tsunami) with an opposite-shore run up height of 85 ± 17 m. The 3100-yr BP deposit has been undisturbed by subsequent events, but progressive offset of the three earlier megaturbidite layers by the Lake Creek – Boundary Creek and Sadie Creek faults beneath the north basin of Lake Crescent suggests that their deposition is related to surface rupturing earthquakes along the fault zone.

The existence of megaturbidites and rockslide deposits in and around Lake Crescent present a substantial seismic hazard for the north-central Olympic Peninsula. There is

significant evidence that the last megaturbidite was sourced by an onshore rockslide entering the lake as a result of an earthquake on the Lake Creek – Boundary Creek fault zone. The volumetric estimate of the subaqueous portion of the rock slide indicates that the resultant maximum displacement wave run up height on the shore opposite to Sledgehammer Point would be approximately 66 to 106 m. A wave of that size would be devastating to the small community of ~150 houses, two resorts, National Park facilities (campgrounds, picnic areas, and scenic pull-outs along Highway 101) that are scattered along the perimeter of the lake. In addition, it would almost certainly dismantle significant portions of U.S. Highway 101 which wraps around Lake Crescent's eastern and southern shores. More than 200 people in Norway have died from inundation caused by subaerial slide generated displacement waves (Blikra et al. 2005). If an event similar to the Sledgehammer Point rockslide-displacement wave were to occur during the peak visitation season at Lake Crescent, there could be hundreds of lives lost. Because of the small size of Lake Crescent, warning times would be short after an event was triggered.

The presence of at least four megaturbidites in the sedimentary record from Lake Crescent indicates that repeated disastrous events have occurred in the past 8,500 years with the most recent dating to 3100 cal yr BP; consequently the lake is possibly overdue for another devastating event, if these events are related to the Lake Creek Boundary Creek fault and its slip behavior is at all quasi-periodic. Assuming the quasi-periodic recurrence of an event on the Lake Creek-Boundary Creek fault, the time elapsed since the most recent 3140 cal yr BP event and the average inter-event time are important for estimating the probabilistic hazard. The median ages of the megaturbidites were used to construct a lognormal distribution model for the probability of an earthquake on the LCBCFZ at Lake Crescent in the next 50 years. Given the data set of four megaturbidite ages and the inter-event times of 900 (x2) and 2300 years, the time-dependent earthquake probability of an event occurring in the next 50 years on the LCBCFZ at Lake Crescent is estimated at 5%.

References Cited in Report

Antinao, J.L., and Gosse, J., 2009, Large rockslides in the Southern Central Andes of Chile (32–34.5 S): Tectonic control and significance for Quaternary landscape evolution: Geomorphology, v. 104, p. 117-133.

Bouma, A.H., 1987, Megaturbidite: an acceptable term?: Geo-Marine Letters, v. 7, p. 63-67.

Brandon, M.T., and Calderwood, A.R., 1990, High-pressure metamorphism and uplift of the Olympic subduction complex: Geology, v. 18, p. 1252-1255.

Brandon, M.T., Roden-Tice, M.K., and Garver, J.L., 1998, Late Cenozoic exhumation of the Cascadia accretionary wedge in the Olympic Mountains, NW Washington State: Geological Society of America Bulletin, v. 110, p. 985-1009.

Brenkman, S.J., Duda, J.J., Kennedy, P.R., and Baker, B.M., 2014, A legacy of divergent fishery management regimes and the resilience of rainbow and cutthroat trout populations in Lake Crescent, Olympic National Park, Washington: Northwest Science, v. 88, p. 280-304.

Brocher, T.M., Parsons, T., Blakely, R.J., Christensen, N.I., Fisher, M.A., and Wells, R.E., 2001, Upper crustal structure in Puget Lowland, Washington: Results from the 1998 seismic hazards investigation in Puget Sound: Journal of Geophysical Research: Solid Earth (1978–2012), v. 106, p. 13541-13564.

Brown, R.D., Jr., Gower, H.D., and Snavely, P.D., Jr., 1960, Geology of the Port Angeles–Lake Crescent area, Clallam County, Washington, Oil and Gas Investigations Map OM-203: Washington, D.C., U.S. Geological Survey.

Clark, E.E., 1953, Indian legends of the Pacific Northwest: Berkeley, University of California Press, 219 p.

Clark, K., Upton, P., Carey, J., Rosser, B., and Strong, D., 2015, Tsunami and Seiche Hazard Scoping Study for Lakes Tekapo, Pukaki, Ohau, Alexandrina and Ruataniwha: GNS Science Consultancy Report 2014, v. 227, p. 82.

Clowes, R.M., Baird, D.J., and Dehler, S.A., 1997, Crustal structure of the Cascadia subduction zone, southwestern British Columbia, from potential field and seismic studies: Canadian Journal of Earth Sciences, v. 34, p. 317-335.

DeMets, C., and Dixon, T.H., 1999, New kinematic models for Pacific-North America motion from 3 Ma to present, I: Evidence for steady motion and biases in the NUVEL-1A Model: Geophysical Research Letters, v. 26, p. 1921-1924.

Dethier, D., Pessl, F., Keuler, R., Balzarini, M., and Pevear, D., 1995, Late Wisconsinan glaciomarine deposition and isostatic rebound, northern Puget Lowland, Washington: Geological Society of America Bulletin, v. 107, p. 1288-1303.

Dragovich, J.D., Logan, R.L., Schasse, H.W., Walsh, T.J., Lingley Jr, W.S., Norman, D.K., Gerstel, W.J., Lapen, T.J., Schuster, J.E., and Meyers, K., 2002, Geologic map of Washington—Northwest

Quadrant, GM-50: Olympia, Washington Department of Natural Resources - Division of Geology and Earth Resources.

Engebretson, D.C., 1985, Relative motions between oceanic and continental plates in the Pacific basin, Geological society of America Special Paper, v. 206, 56 p.

Evers, F.M., and Hager, W.H., 2016, Spatial impulse waves: wave height decay experiments at laboratory scale: Landslides, p. 1-9.

Fritz, H.M., Mohammed, F., and Yoo, J., 2009, Lituya Bay landslide impact generated mega-tsunami 50th anniversary: Pure and Applied Geophysics, v. 166, p. 153-175.

Gomberg, J., and Sherrod, B., 2014, Crustal earthquake triggering by modern great earthquakes on subduction zone thrusts: Journal of Geophysical Research: Solid Earth, v. 119, p. 1235-1250.

Haugerud, R., 2002, Lidar evidence for Holocene surface rupture on the Little River fault near Port Angeles, Washington [abstract]: Seismological Research Letters, Volume 73, p. 249.

Haugerud, R.A., Harding, D.J., Johnson, S.Y., Harless, J.L., Weaver, C.S., and Sherrod, B.L., 2003, High-resolution lidar topography of the Puget Lowland, Washington—A Bonanza for Earth Science: GSA Today, v. 13, p. 4-10.

Heller, V., Hager, W., and Minor, H., 2009, Landslide generated impulse waves in reservoirs: Basics and computation, Mitteilungen 211, Zurich: VAW, ETH Zurich.

Heller, V., and Spinneken, J., 2015, On the effect of the water body geometry on landslide–tsunamis: Physical insight from laboratory tests and 2D to 3D wave parameter transformation: Coastal Engineering, v. 104, p. 113-134.

Heusser, C.J., 1973, Environmental sequence following the Fraser advance of the Juan de Fuca lobe, Washington: Quaternary Research, v. 3, p. 284-306.

Hilbe, M., and Anselmetti, F.S., 2014, Signatures of slope failures and river-delta collapses in a perialpine lake (Lake Lucerne, Switzerland): Sedimentology, v. 61, p. 1883-1907.

Hovius, N., Meunier, P., Lin, C.-W., Chen, H., Chen, Y.-G., Dadson, S., Horng, M.-J., and Lines, M., 2011, Prolonged seismically induced erosion and the mass balance of a large earthquake: Earth and Planetary Science Letters, v. 304, p. 347-355.

Howarth, J.D., Fitzsimons, S.J., Norris, R.J., and Jacobsen, G.E., 2012, Lake sediments record cycles of sediment flux driven by large earthquakes on the Alpine fault, New Zealand: Geology.

Hyndman, R., Mazzotti, S., Weichert, D., and Rogers, G., 2003, Frequency of large crustal earthquakes in Puget Sound–Southern Georgia Strait predicted from geodetic and geological deformation rates: Journal of Geophysical Research: Solid Earth (1978–2012), v. 108.

Joyner, C.N., 2016, Lacustrine Megaturbidites and Displacement Waves: The Holocene Earthquake History of the Lake Creek-Boundary Creek Fault at Lake Crescent, Washington, USA: North Carolina State University Master's Thesis, p. 187.

Keefer, D.K., 1984, Landslides caused by earthquakes: Geological Society of America Bulletin, v. 95, p. 406-421.

Keefer, D.K., 2002, Investigating landslides caused by earthquakes–a historical review: Surveys in geophysics, v. 23, p. 473-510.

Kelts, K., Briegel, U., Ghilardi, K., and Hsu, K., 1986, The limnogeology-ETH coring system: Swiss journal of hydrology, v. 48, p. 104-115.

Larsen, I.J., Montgomery, D.R., and Korup, O., 2010, Landslide erosion controlled by hillslope material: Nature Geoscience, v. 3, p. 247-251.

Logan, R.L., and Schuster, R.L., 1991, Lakes divided: The origin of Lake Crescent and Lake Sutherland, Clallam County, Washington: Wash. Geol, v. 19, p. 38-42.

Ludwin, R.S., Smits, G.J., Carver, D., James, K., Jonientz-Trisler, C., McMillan, A., Losey, R., Dennis, R., Rasmussen, J., and De Los Angeles, A., 2007, Folklore and earthquakes: Native American oral traditions from Cascadia compared with written traditions from Japan: Geological Society, London, Special Publications, v. 273, p. 67-94.

Mackey, B.H., Roering, J.J., and Lamb, M.P., 2011, Landslide-dammed paleolake perturbs marine sedimentation and drives genetic change in anadromous fish: Proceedings of the National Academy of Sciences of the United States of America, v. 108, p. 18905-18909.

Mazzotti, S., Dragert, H., Hyndman, R.D., Miller, M.M., and Henton, J.A., 2002, GPS deformation in a region of high crustal seismicity: N. Cascadia forearc: Earth and Planetary Science Letters, v. 198, p. 41-48.

McCaffrey, R., Qamar, A.I., King, R.W., Wells, R., Khazaradze, G., Williams, C.A., Stevens, C.W., Vollick, J.J., and Zwick, P.C., 2007, Fault locking, block rotation and crustal deformation in the Pacific Northwest: Geophysical Journal International, v. 169, p. 1315-1340.

Meyer, J., and Fradkin, S., 2002, Summary of fisheries and limnological data for Lake Crescent, Washington: Olympic National Park Report, National Park Service, Port Angeles, WA.

Moernaut, J., Daele, M.V., Heirman, K., Fontijn, K., Strasser, M., Pino, M., Urrutia, R., and De Batist, M., 2014, Lacustrine turbidites as a tool for quantitative earthquake reconstruction: New evidence for a variable rupture mode in south central Chile: Journal of Geophysical Research: Solid Earth, v. 119, p. 1607-1633.

Morell, K.D., Regalla, C., Leonard, L.J., Amos, C., and Levson, V., 2017, Quaternary rupture of a crustal fault beneath Victoria, British Columbia, Canada: GSA Today, v. 27, p. 4-10.

Nelson, A.R., Personius, S.F., Buck, J., Bradley, L.-A., Wells, R.E., and Schermer, E.R., 2007, Field and laboratory data from an earthquake history study of scarps of the Lake Creek-Boundary Creek fault between the Elwha River and Siebert Creek, Clallam County, Washington: U.S. Geological Survey Scientific Investigations Map 2961, 2 sheets.

Nelson, A.R., Personius, S.F., Wells, R.E., Bradley, L.-A., Buck, J., Schermer, E.R., and Reitman, N., in press, Holocene earthquakes of magnitude 7 during westward escape of the Olympic Mountains, Washington: Bulletin of the Seismological Society of America.

Olsson, L., 1986, Radiometric methods, *in* Berglund, B., ed., Handbook of Holocene Palaeoecology and Palaeohydrology: Chichester, John Wiley & Sons, p. 273-312.

Parker, R.N., Densmore, A.L., Rosser, N.J., de Michele, M., Li, Y., Huang, R., Whadcoat, S., and Petley, D.N., 2011, Mass wasting triggered by the 2008 Wenchuan earthquake is greater than orogenic growth: Nature Geosci, v. 4, p. 449-452.

Pazzaglia, F.J., and Brandon, M.T., 2001, A fluvial record of rock uplift and shortening across the Cascadia forearc high: American Journal of Science, v. 301, p. 385-431.

Pierce, B.E., 1984, The trouts of Lake Crescent, Washington [M.S. Thesis]: Colorado State Univesity, 252 p.

Polenz, M., Wegmann, K.W., and Schasse, H.W., 2004, Geologic map of the Elwha and Angeles Point 7.5-minute quadrangles, Clallam County, Washington: Washington Division of Geology and Earth Resource Open File Report 2004-14, 1 sheet, scale 1:24,000 [http://www.dnr.wa.gov/geology/pdf/ofr04-14.pdf].

Pollen, A.F., 2016, The Sedimentary Record of Past Earthquakes Identified in Holocene Sediments of Lake Crescent, Washington: Raleigh, North Carolina State University.

Pringle, P., Wegmann, K., Pontbriand, D., and Walker, W.W., 2010, Some recent discoveries pertaining to subfossil forests in the Pacific Northwest—Examples from Lake Crescent and Lower Dry Beds Lakes, Olympic Mountains, Washington: Northwest Scientific Association, Annual Meeting, v. 82, p. 77-78.

Ramsey, C.B., 2009, Bayesian analysis of radiocarbon dates: Radiocarbon, v. 51, p. 337-360.

Reimer, P.J., Bard, E., Bayliss, A., Beck, J.W., Blackwell, P.G., Bronk Ramsey, C., Buck, C.E., Cheng, H., Edwards, R.L., and Friedrich, M., 2013, IntCal13 and Marine13 radiocarbon age calibration curves 0-50,000 years cal BP: Radiocarbon, v. 55, p. 1869-1887.

Roberts, N.J., McKillop, R.J., Lawrence, M.S., Psutka, J.F., Clague, J.J., Brideau, M.-A., and Ward, B.C., 2013, Impacts of the 2007 landslide-generated tsunami in Chehalis Lake, Canada, Landslide science and practice, Springer, p. 133-140.

Sassa, K., and Canuti, P., 2009, Landslides-Disaster Risk Edition: Berlin Heidelberg, Germany, Springer, p. 648.

Schasse, H.W., 2003, Geologic map of the Washington portion of the Port Angeles 1:100,000 quadrangle: Washington Division of Geology and Earth Resources Open File Report 2003-6.

Schasse, H.W., and Wegmann, K.W., 2000, Geologic map of the Carlsborg 7.5-minute quadrangle, Clallam County, Washington.

Schasse, H.W., Wegmann, K.W., and Polenz, M., 2004, Geologic map of the Port Angeles and Ediz Hook 7.5-minute quadrangles, Clallam County, Washington: Washington Division of Geology and Earth Resource Open File Report 2004-13, 1 sheet, scale 1:24,000 [http://www.dnr.wa.gov/geology/pdf/ofr04-13.pdf].

Schnellmann, M., Anselmetti, F.S., Giardini, D., McKenzie, J.A., and Ward, S.N., 2002, Prehistoric earthquake history revealed by lacustrine slump deposits: Geology, v. 30, p. 1131-1134.

Sherrod, B., and Gomberg, J., 2014, Crustal earthquake triggering by pre-historic great earthquakes on subduction zone thrusts: Journal of Geophysical Research: Solid Earth, p. 2013JB010635.

Tabor, R.W., 1975, Guide to the geology of Olympic National Park: Seattle, University of Washington Press, 144 p.

Tabor, R.W., and Cady, W.M., 1978a, Geologic map of the Olympic Peninsula: U.S. Geological Survey Map I-994, 2 sheets, scale 1:125,000.

Tabor, R.W., and Cady, W.M., 1978b, The structure of the Olympic Mountains, Washington—Analysis of a subduction zone: U.S. Geological Survey Professional Paper 1033, 39 p.

U.S. Geological Survey, 2001, Clallam County: Mount Muller, Lake Crescent, Lake Sutherland http://gis.ess.washington.edu/data/raster/tenmeter/byquad/index.html (accessed June 2016).

Van Daele, M., Moernaut, J., Doom, L., Boes, E., Fontijn, K., Heirman, K., Vandoorne, W., Hebbeln, D., Pino, M., and Urrutia, R., 2015, A comparison of the sedimentary records of the 1960 and 2010 great Chilean earthquakes in 17 lakes: Implications for quantitative lacustrine palaeoseismology: Sedimentology.

Wegmann, K.W., Bohnenstiehl, D.R., Bowman, J.D., Homburg, J.A., Windingstad, J.D., and Beery, D., 2012, Assessing Coastal Landscape Change for Archaeological Purposes: Integrating Shallow Geophysics, Historical Archives and Geomorphology at Port Angeles, Washington, USA: Archaeological Prospection, v. 19, p. 229-252.

Wegmann, K.W., Leithold, E.L., and Bohnenstiehl, D.R., 2014a, How important is seismically-induced erosion above the Cascadia subduction zone? Insights from the stratigraphy of large lakes on the Olympic Peninsula, Washington State, *in* Gillespie, A., and Montgomery, D., eds., Proceedings of the 23rd Biennial Meeting of the American Quaternary Association, Volume 23: University of Washington, Seattle, WA, American Quaternary Union, p. 35-37.

Wegmann, K.W., Bohnenstiehl, D.R., Leithold, E.L., and Pringle, P.T., 2014b, Earthquakes, mass wasting, and fish from northern Cascadia: Post-glacial rupture of the lake Creek-Boundary Creek Fault revealed by Chirp seismic investigations at Lake Crescent, Washington: Geological Society of America Abstracts with Programs, v. 46, p. 779.

Wells, R.E., and McCaffrey, R., 2013, Steady rotation of the Cascade arc: Geology, v. 41, p. 1027-1030.

Wells, R.E., and Simpson, R.W., 2001, Northward migration of the Cascadia forearc in the northwestern US and implications for subduction deformation: Earth Planets and Space, v. 53, p. 275-284.

Wells, R.E., Weaver, C.S., and Blakely, R.J., 1998, Fore-arc migration in Cascadia and its neotectonic significance: Geology, v. 26, p. 759-762.

Willett, S.D., and Brandon, M.T., 2002, On steady states in mountain belts: Geology, v. 30, p. 175-178.

Publications Resulting from the Work Performed as of May, 2017

Leithold, E.L., Wegmann, K.W., Bohnenstiehl, D.R., Pollen, A.F., and Joyner, C., 2016, Megaturbidites in Lake Crescent, Washington—Sedimentary record of repeated catastrophic events triggered by surface rupture of the Lake Creek–Boundary Creek fault: Geological Society of America Abstracts with Programs, v. 48.

Joyner, C.N, 2016, Lacustrine Megaturbidites and Displacement Waves: The Holocene Earthquake History of the Lake Creek–Boundary Creek Fault at Lake Crescent, Washington, USA: North Carolina State University Master's Thesis, 187 p; http://www.lib.ncsu.edu/resolver/1840.20/33332

Pollen, A.F., 2016, The Sedimentary Record of Past Earthquakes Identified in Holocene Sediments of Lake Crescent, Washington [M.S. Thesis]: North Carolina State University, 79 p; http://www.lib.ncsu.edu/resolver/1840.16/11366

Thackray, G., Gavin, D., Ritchie, A., Wegmann, K., Ashworth, A., and Ely, L., 2015, Late Pleistocene to Modern Geomorphic and Biotic History of the Olympic Peninsula, Washington: Friends of the Pleistocene, Pacific Northwest Cell Field Trip September 17-20, 2015, 121 p.; http://www.fop.cascadiageo.org/pacific_northwest_cell/2015/FOP_PNW_2015_Olympic_field_guide.pdf

Wegmann, K.W., Leithold, E.L., Bohnenstiehl, D.R., Joyner, C.N., and Pollen, A.F., 2016, Holocene earthquakes, rockslides, tsunamis, and fish: Cascadia forearc convergence and rotation accommodated by seismogenic faulting along the Lake Creek–Boundary Creek fault, Olympic Peninsula, Washington State, U.S.A., Annual Meeting of the Geophysical Union of Mexico, Abstracts with Program: Puerto Vallarta, Mexico, Mexican Geophysical Union, p. SE01-4.